Comprehensive Virtual Screening of the Antiviral Potentialities of Marine Polycyclic Guanidine Alkaloids against SARS-CoV-2 (Covid-19)

Amr El-Demerdash[1,2,*], Ahmed M. Metwaly[3,*], Tarek Mohamed Abd El-Aziz[4,5], Ibrahim H. Eissa[6] and James D. Stockand[4,*]

[1]Institut de Chimie des Substances Naturelles, CNRS UPR 2301, Université Paris-Sud, Université Paris-Saclay, 1, Avenue de la Terrasse, 91198 Gif-sur-Yvette, France.

[2]Organic Chemistry Division, Chemistry Department, Faculty of Science, Mansoura University, Mansoura 35516, Egypt.

[3]Pharmacognosy Department, Faculty of Pharmacy (Boys), Al-Azhar University, Cairo 11884, Egypt.

[4]Department of Cellular and Integrative Physiology, University of Texas Health Science Center at San Antonio, San Antonio, TX 78229-3900, USA.

[5]Zoology Department, Faculty of Science, Minia University, El-Minia 61519, Egypt.

[6]Pharmaceutical Medicinal Chemistry & Drug Design Department, Faculty of Pharmacy (Boys), Al-Azhar University, Cairo 11884, Egypt.

ABSTRACT: A comprehensive *in silico* binding affinity of fifteen guanidine alkaloids against five different proteins of SARS-CoV-2 has been investigated. The investigated proteins are COVID-19 main protease (M^{pro}) (PDB ID: 6lu7), spike glycoprotein (PDB ID: 6VYB), nucleocapsid phosphoprotein (PDB ID: 6VYO), membrane glycoprotein (PDB ID: 6M17), and non-structural protein (nsp10) (PDB ID: 6W4H). The binding energies for all tested compounds indicated promising binding affinities. A noticeable superiority for the pentacyclic alkaloids particularly, crambescidin 786 (**5**) and crambescidin 826 (**13**) have been observed. Compound **5** exhibited very good binding affinities against M^{pro} (ΔG = -8.05 kcal/mol), nucleocapsid phosphoprotein (ΔG = -6.49 kcal/mol), and nsp10 (ΔG = -9.06 kcal/mol). Compound **13** showed promising binding affinities against M^{pro} (ΔG = -7.99 kcal/mol), spike glycoproteins (ΔG = -6.95 kcal/mol), and nucleocapsid phosphoprotein (ΔG = -8.01 kcal/mol). Such promising activities might be attributed to the long ω-fatty acid chain, which may play a vital role in binding within the active sites. The ADMET studies were carried out *in silico* for the 15 compounds, all examined compounds (except compounds **8** and **15**) have low or very low BBB penetration levels. Compounds **1**, **5**, **6**, **9**, **12** and **13** showed optimal range levels of ADMET aqueous solubility. Compounds **1**, **2**, **3**, **8**, and **15** were predicted to have good intestinal absorption levels, while compounds **4**, **7**, **9**, **10**, and **14** showed moderate absorption levels. All examined alkaloids (except the bicyclic compound **8**) were predicted not to be inhibitors of CYP2D6, non-hepatotoxic, and bind plasma protein with a percentage less than 90%. The toxicity of the tested compounds was screened *in silico* against five models (FDA rodent carcinogenicity, carcinogenic potency TD_{50}, rat maximum tolerated dose, rat oral LD_{50} and rat chronic LOAEL). All compounds showed expected low toxicity against the tested models.

Keywords: Virtual screening; Docking; Covid-19; Antiviral; Cytotoxicity; Guanidine Alkaloids, Crambescidines, Crambescins; *Monanchora* n. sp.

INTRODUCTION

Covid-19 is a disease caused by a new strain of the Coronavirus. This disease first appeared in Wuhan, China at the end of December 2019. Two months later, the disease became widespread in China [1, 2]. Covid-19 has now turned into a pandemic affecting almost every country in the world. As of December 1, 2020, COVID-19 has affected more than 63,697,245 patients in more than 188 countries and territories around the world and caused around 1,477,645 deaths worldwide. Unfortunately, there is no specific antiviral medications available for treatment of COVID-19 patients. Many scientists worldwide are working to prepare a vaccine to fight COVID-19 infection. At present, several vaccines have been approved for clinical trials at home and abroad.

Coronaviruses viruses belong to the order *Nidovirales* in the subfamily *Coronavirinae* (family Coronaviridae) [3]. They are enveloped viruses that contain a large non-segmented, positive-sense RNA genome with a length of up to 33.5 kilobases [4]. The Coronaviridae family can be classified into four genera to include Alpha-, Beta-, Gamma- and Delta-coronavirus (alphaCoV, betaCoV, gammaCoV and deltaCoV). Coronaviruses were named for how they appear under the electron microscope. The viruses look like they are covered with pointed structures that surround them like a corona or crown due to the presence of spike glycoproteins on their envelope (**Figure 1**) [5].

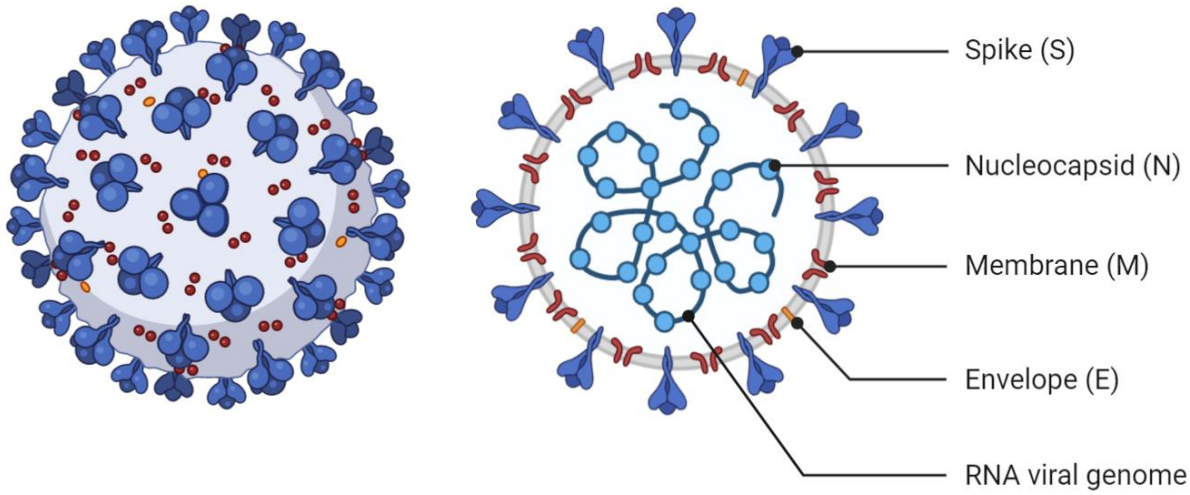

Figure 1. Schematic representation of the structure of SARS-CoV-2. It has at least four canonical structural proteins; E (envelope), M (membrane), N (nucleocapsid) and S (spike) proteins (Created with BioRender.com).

Coronaviruses mostly cause insignificant respiratory infections, including the common cold. However, more recent emerging coronaviruses can cause more serious diseases, including severe acute respiratory syndrome (SARS-CoV) and Middle East respiratory syndrome (MERS-CoV) [6, 7]. SARS-CoV and MERS-CoV are caused by zoonotic coronaviruses that belong to the betaCoV genus. Bats and rodents are thought to be the reservoir for alphaCoV and betaCoV. SARS-CoV detected first in 2002 in Foshan, China, possibly originated from the Chinese horseshoe bat-CoV, 35 to 20 years ago via zootonic transmission from the civet [8-11]. MERS-CoV detected in 2012 in the Arabian Peninsula, possibly originated from the South African Bat-CoV, around 14 years ago via zootonic transmission from the camel [8, 9, 12]. SARS-CoV-2 detected in 2019 in Wuhan, China, possibly originated the from intermediate horseshoe bat-CoV around 11 years ago via zootonic transmission from pangolins [13-15].

Generally, viral proteins can be classified according to their functions into two major groups as structural and non-structural proteins [16]. Structural proteins, such as nucleocapsid proteins, can function as shields protecting viral DNA from being degrading by host enzymes [17]. Other vital structural proteins are the membrane glycoproteins which form an envelope enclosing the virus capsid and bind to specific receptors on host cell membranes [18]. For example, the coronavirus spike glycoprotein (S protein) by binding to a specific cellular receptor is a significant structural protein that mediates entry into cells [19]. The main protease (Mpro) is a key non-structural chymotrypsin-like cysteine proteases enzyme used by coronaviruses for replication. It acts on the two large polyproteins (PP1a and PP1ab) to release the 16 non-structural proteins (NSPs 1-16) through cleavage of the C-terminal end of these PPs [20, 21]. The non-structural protein (NSP10) by functioning as a vital cofactor is a crucial regulator of the replicative enzyme SARS-CoV replicas [22].

Given the fact that oceans and seas cover almost 70% of the earth and consequently, contain the largest ecological diversity of biological species, marine natural products (MNPs) attract much interests. This includes metabolite congers from the marine sponge *Cryptotethya crypta* [23]. MNPs, many of which have distinct structures and biological mechanism of actions, represent a huge renewable natural reservoir for possible new drugs [24-35]. Among the eight clinically approved marine drugs, two successful molecules were identified as antiviral drugs, namely cytarabine (Cytosar-U®, Depocyt®) and vidarabine (Vira-A®). These are synthetic analogues originally inspired by spongothymidine, which is the first nucleoside isolated from

the sponge *Cryptotethya crypta*. Both compounds hinder viral DNA polymerase and consequently, DNA synthesis in particular *herpes simplex* virus type 1 and type 2, vaccinia and varicella zoster viruses [26]. Additionally, two marine-derive molecules are being pre-clinically investigated for their antiviral-HIV-1, HIV-2, SIV activities. These are avarol, a sesquiterpenoid hydroquinone isolated from the marine sponge *dysidea avara*, and cyanovirin-N, a protein isolated from cultures of the cyanobacterium (blue-green alga) *Nostoc ellipsosporu* [36]. Meanwhile, recent synthetic efforts and clinical trials highlight the exploration of an additional 19 structurally divergent MNP, many of which are nucleosides, as antivirals [37].

Polycyclic guanidine alkaloids (PGAs) represent a major group of marine metabolites common to Poecilosclerida sponges including *Batzella*, *Crambe*, *Monanchora*, *Clathria*, *Ptilocaulis*, ; and some starfishes, such as *Fromia monilis* and *Celerina heffernani* [38-40]. Since the discovery of the first antiviral pentacyclic congener, ptilomycalin A, in 1989 by Kashman and co-workers [41], these metabolites have attracted much interest. Chemically, PGAs contain a common central tricyclic guanidinic core (*Vessel*) linked to a ω-long chain fatty acid (*Anchor*). They are synthesized via the Aza-Michael incorporation of a polyketide chain with a guanidinic moiety, followed by subsequent cyclizations, substitutions and oxidations. These chemical reactions produce a structurally complex and diverse group of molecules that have a central guanidinic core, including bicyclic (e.g. crambescins), tricyclic (e.g. batzelladines) and pentacyclic (e.g. crambescidines) derivatives [38-42]. PGA metabolites are recognized for displaying a broad spectrum of biomedical properties, including being cytotoxicity [43-50], antimicrobial [51,52], antifungal [53,54], antimalarial and anti-infective [55-58]; as well as being enzyme inhibitors and Ca+2 channel blockers [59,60]. Moreover, many PGAs have been reported to display significant antiviral activities against HIV-1, *herpes simplex* type-1 [41,43,61-67]. Indeed, polycyclic guanidinic meltabilities including tricyclic batzelladines and pentacyclic crambescidins isolated from the marine sponges *Crambe crambe* and *Monanchora unguifera* and their synthetic analogues displayed significant inhibitory activity against gp120-CD4 binding, motivate CD4-p56lck dissociation and prevent HIV-1 cell fusion [68-71].

As part of our research into MNPs together with the global effort to find new robust antiviral drugs capable of combating Covid-19, we report here on the potential interactions between five SARS-CoV-2 proteins and fifteen structurally divers polycyclic guanidine-containing alkaloids isolated from the Pacific marine sponge *Monanchora* n. sp. [45].

RESULTS AND DISCUSSION

In this work, the binding potential of 15 guanidine-containing marine alkaloids (**1-15**), previously isolated from the French Polynesian *Monanchora* n. sp marine sponge (**Chart 1**), against a host of SARS-CoV-2 proteins has been investigated. Five SARS-CoV-2 proteins (structural and non-structural) were selected. These include : i) the COVID-19 main protease (M^{pro}) (PDB ID: 6lu7, resolution: 2.16 Å), ii) the spike glycoproteins (PDB ID: 6VYB, resolution: 3.20 Å), iii) the nucleocapsid phosphoprotein (PDB ID: 6VYO, resolution: 1.70 Å), iv) the membrane glycoprotein (PDB ID: 6M17, resolution: 2.90 Å), and v) the nonstructural protein (nsp)10 (PDB ID: 6W4H, resolution: 1.80 Å). Comprehensive docking studies were performed using MOE14.0 software. These docking studies predicted the free energy (ΔG) of binding specifically for the molecules shown in **Figure 2**.

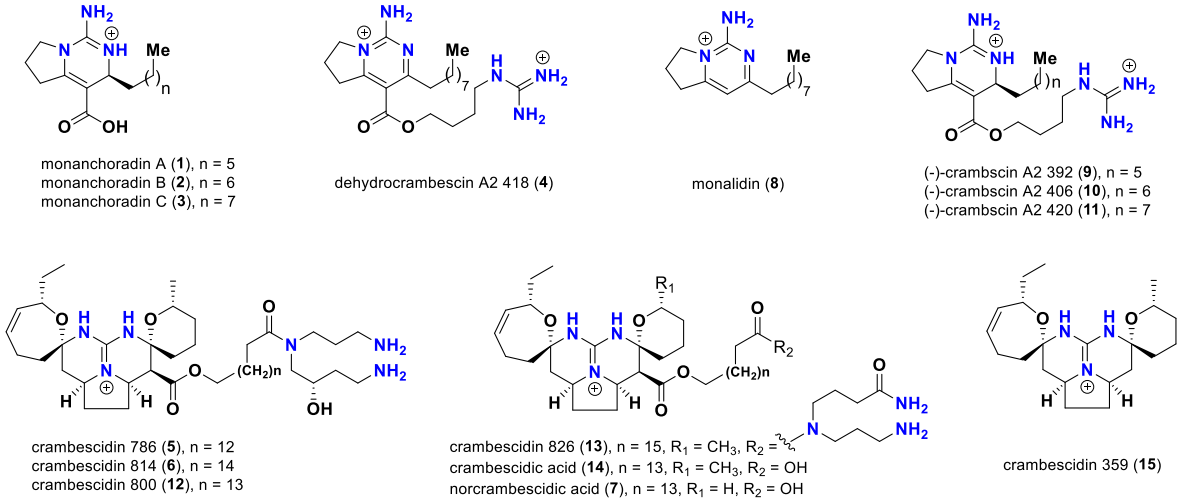

Chart 1. Reported polycyclic guanidine alkaloids (**1-15**) from *Monanchora* n. sp. marine sponge.

Docking studies showed in general robust binding energies for all compounds tested with a noticeable superiority for pentacyclic compounds. The pentacyclic guanidines, crambescidins 786 (**5**) and 826 (**13**) exhibited the greatest free energy of docking. Crambescidin 786 (**5**) showed promising binding affinities against COVID-19 main protease (ΔG = -8.05 kcal/mol), nucleocapsid phosphoprotein (ΔG = -6.49 kcal/mol), and nsp10 (ΔG = -9.06 kcal/mol), compared to the co-crystallized ligands PRD_002214 (ΔG = -8.18 kcal/mol), MES (ΔG = -3.80 kcal/mol), and SAM (ΔG = -5.77 kcal/mol), respectively. In addition, crambescidin 826 (**13**)

showed good binding affinities against COVID-19 main protease (ΔG = -7.99 kcal/mol), spike glycoproteins (ΔG = -6.95 kcal/mol), and nucleocapsid phosphoprotein (ΔG = -8.01 kcal/mol), compared to the co-crystallized ligands PRD_002214 (ΔG = -8.18 kcal/mol), NAG (ΔG = -3.56 kcal/mol), and MES (ΔG = -3.80 kcal/mol), respectively (**Table 1**).

Table 1: Free energies of binding for fifteen marine guanidine alkaloids (**1-15**) to SARS-CoV-2 target proteins

Compound	COVID-19 main protease	Spike glycoproteins	Nucleocapsid phosphoprotein	Membrane glycoprotein	NSP10
Monanchoradin A (**1**)	-5.62	-3.83	-4.70	-4.27	-6.12
Monanchoradin B (**2**)	-5.54	-4.10	-4.46	-4.65	-5.73
Monanchoradin C (**3**)	-6.01	-3.71	-5.10	-4.61	-6.08
Dehydrocrambescin A2 418 **(4)**	-6.45	-4.50	-6.31	-5.69	-7.19
Crambescidin 786 (**5**)	-8.05	-5.60	-6.49	-6.37	-9.06
Crambescidin 814 (**6**)	-7.87	-6.87	-6.34	-6.97	-7.50
Norcrambescidic acid (**7**)	-7.50	-5.81	-6.37	-7.34	-7.35
Monalidin (**8**)	-5.77	-3.55	-4.63	-4.32	-5.63
(-)-crambescin A2 392 (**9**)	-6.93	-4.07	-5.47	-5.50	-6.61
(-)-crambescin A2 406 (**10)**	-6.88	-4.60	-5.44	-6.01	-10.54
(-)-crambescin A2 420 (**11)**	-7.38	-4.32	-5.60	-5.61	-6.53
Crambescidin 800 (**12**)	-6.75	-6.49	-6.29	-7.04	-7.22
Crambescidin 826 (**13**)	-7.99	-6.95	-8.01	-6.09	-8.39
Crambescidic acid (**14**)	-7.02	-5.36	-6.05	-6.66	-7.38
Crambescidin 359 (**15**)	5.53	-3.85	-4.55	-4.39	-4.72
Co-crystallized ligand (PRD_002214)	-8.18	-	-	-	-
Co-crystallized ligand (NAG)	-	-3.56	-	-	-
Co-crystallized ligand (MES)	-	-	-3.80	-	-
Co-crystallized ligand (NAG)	-	-	-	-3.63	-
Co-crystallized ligand (SAM)	-	-	-	-	-5.77

The detailed binding mode of the co-crystallized ligand (PRD_002214) against COVID-19 main protease was as follows: the ligand formed four hydrogen bonds and three hydrophobic interactions. In addition, the 2-oxopyrrolidin-3-yl moiety occupied the first pocket of (M^{pro}) and the isopropyl moiety occupied the second pocket of (M^{pro}). Furthermore, the benzyl

172 acetate moiety occupied the third pocket of the receptor. Moreover, the 5-methylisoxazole-3-
173 carboxamide moiety was incorporated in the fourth pocket (**Figure 2**). For the binding mode
174 of the co-crystallized ligand (NAG) against COVID-19 spike glycoprotein, it formed five
175 hydrogen bonds with Asn61, Asn30, The29, and Phe59 (**Figure 3**).
176 Additionally, the co-crystallized ligand (MES) bonded with COVID-19 nucleocapsid
177 phosphoprotein through the formation of two hydrogen bonds with Asn154 and Asn75
178 (**Figure 4**). Furthermore, the co-crystallized ligand (NAG) docked into the active site of
179 COVID-19 membrane glycoprotein showed four hydrogen bonds with Ser390, Ser64, Glu261,
180 and Gln63 (**Figure 5**). Finally, the binding mode of the co-crystallized ligand (SAM) against
181 COVID-19 nsp10 showed three hydrogen bonds with Asn6899, Tyr6930, Asp6928, and
182 Asp6897. Moreover, it formed seven hydrophobic interactions with Lys6968, Lys6844,
183 Asp6928, Phe6947, and Leu6898 (**Figure 6**).
184
185
186

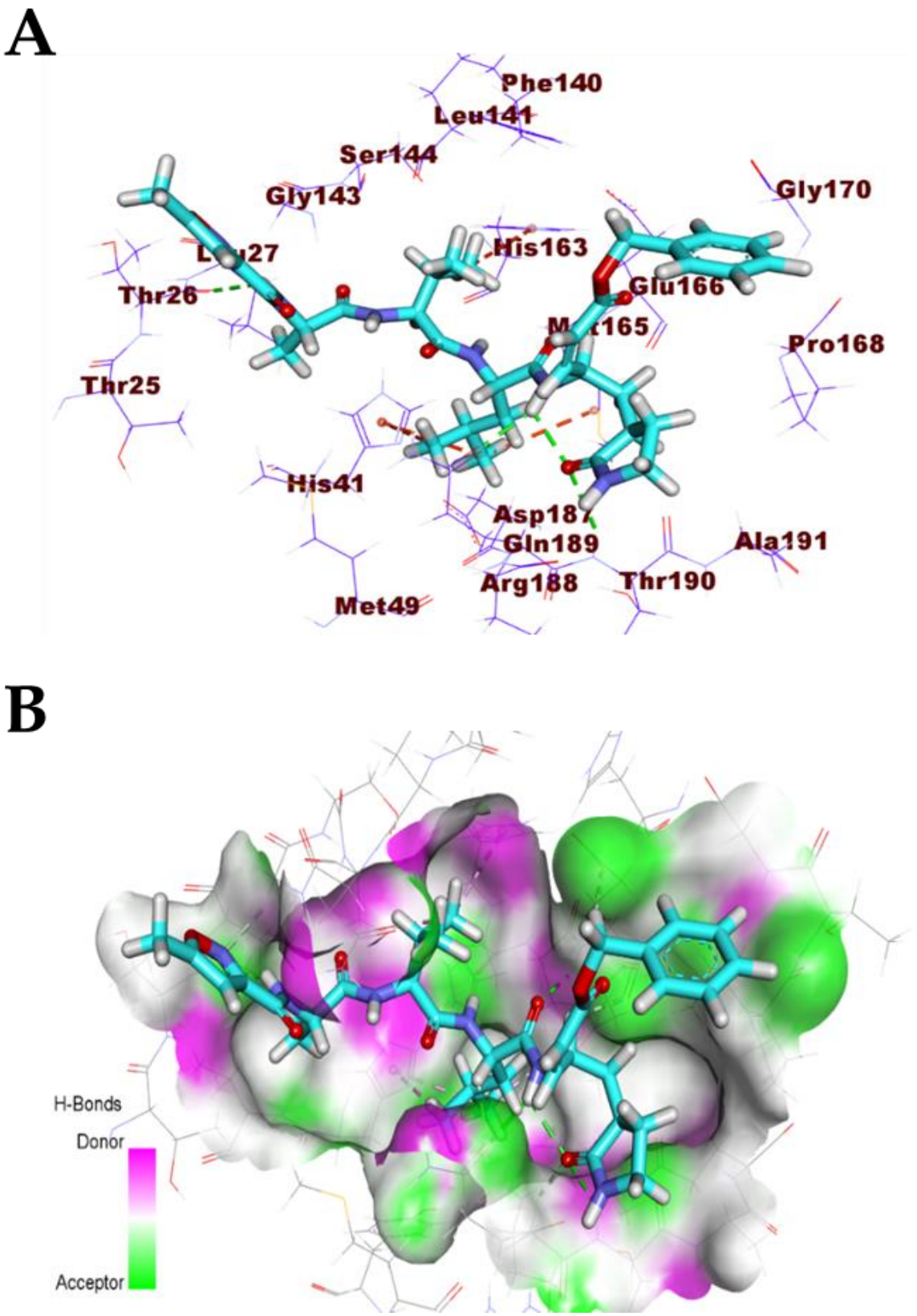

Figure 2. A. Co-crystallized ligand (PRD_002214) docked into the active site of COVID-19 main protease. **B**. Mapping surface showing Co-crystallized ligand (PRD_002214) occupying the active pocket of COVID-19 main protease.

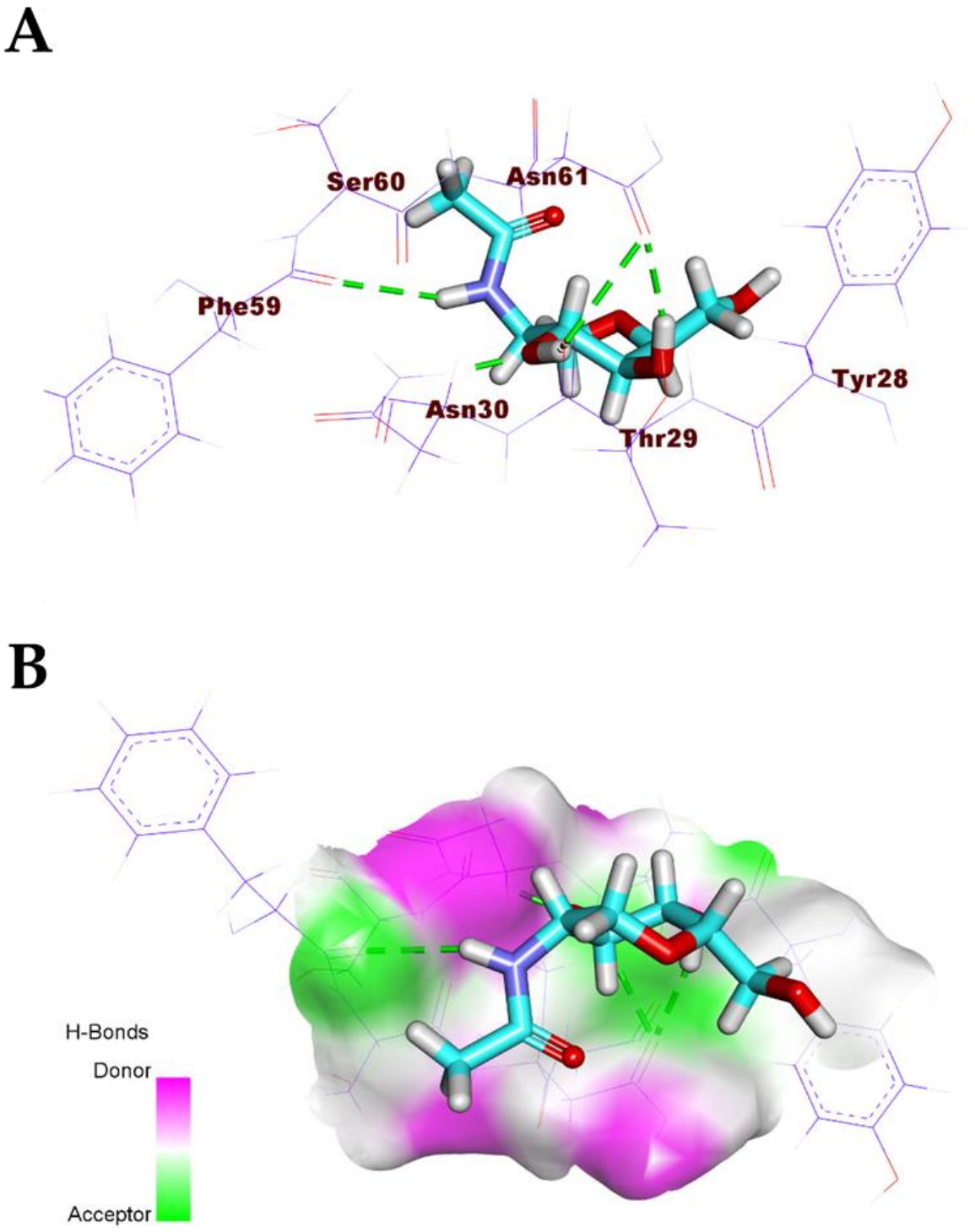

Figure 3. A. Co-crystallized ligand (NAG) docked into the active site of COVID-19 spike glycoprotein. **B.** Mapping surface showing Co-crystallized ligand (NAG) occupying the active pocket of COVID-19 spike glycoproteins.

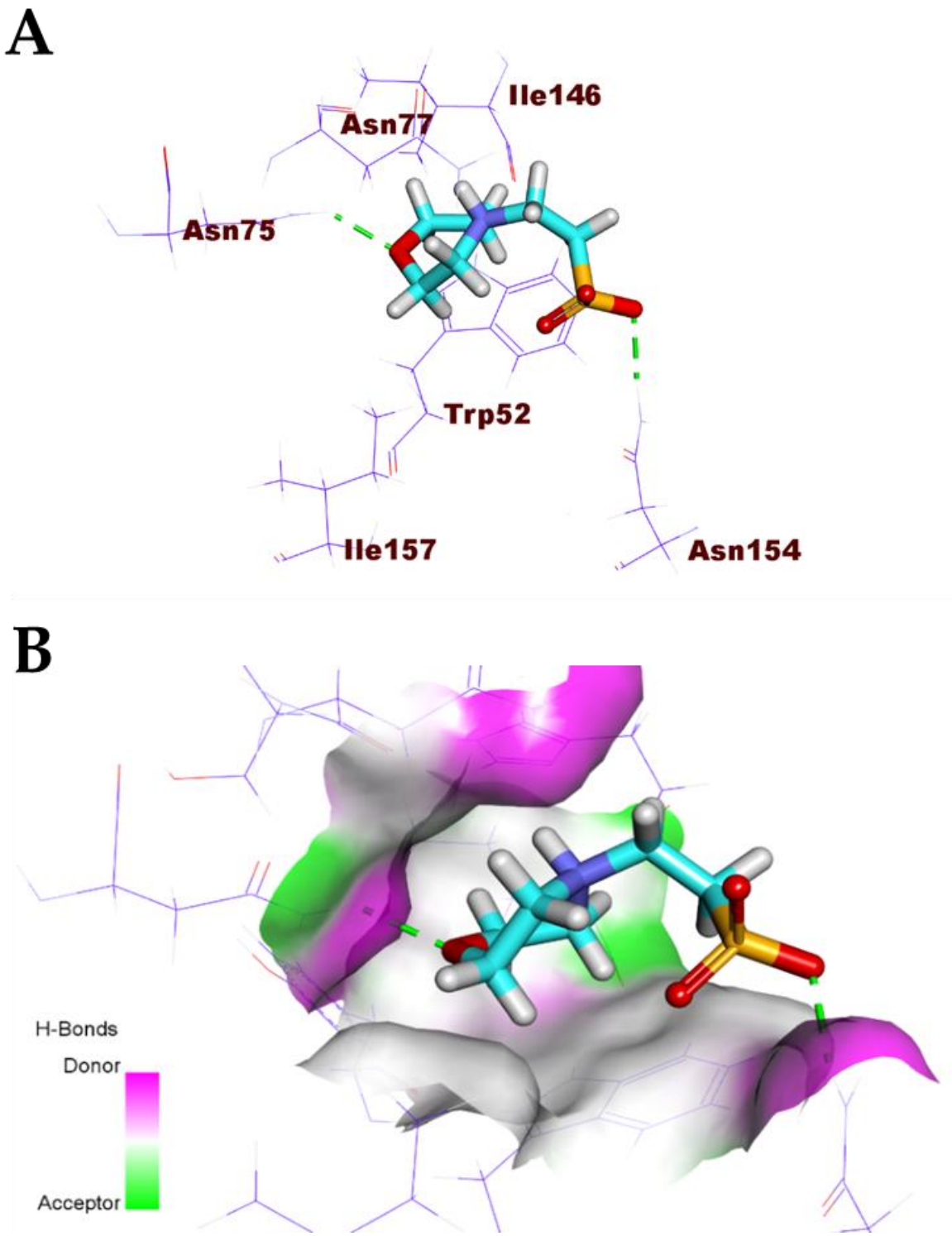

Figure 4. **A.** Co-crystallized ligand (MES) docked into the active site of COVID-19 nucleocapsid phosphoprotein. **B.** Mapping surface showing Co-crystallized ligand (MES) occupying the active pocket of COVID-19 nucleocapsid phosphoprotein.

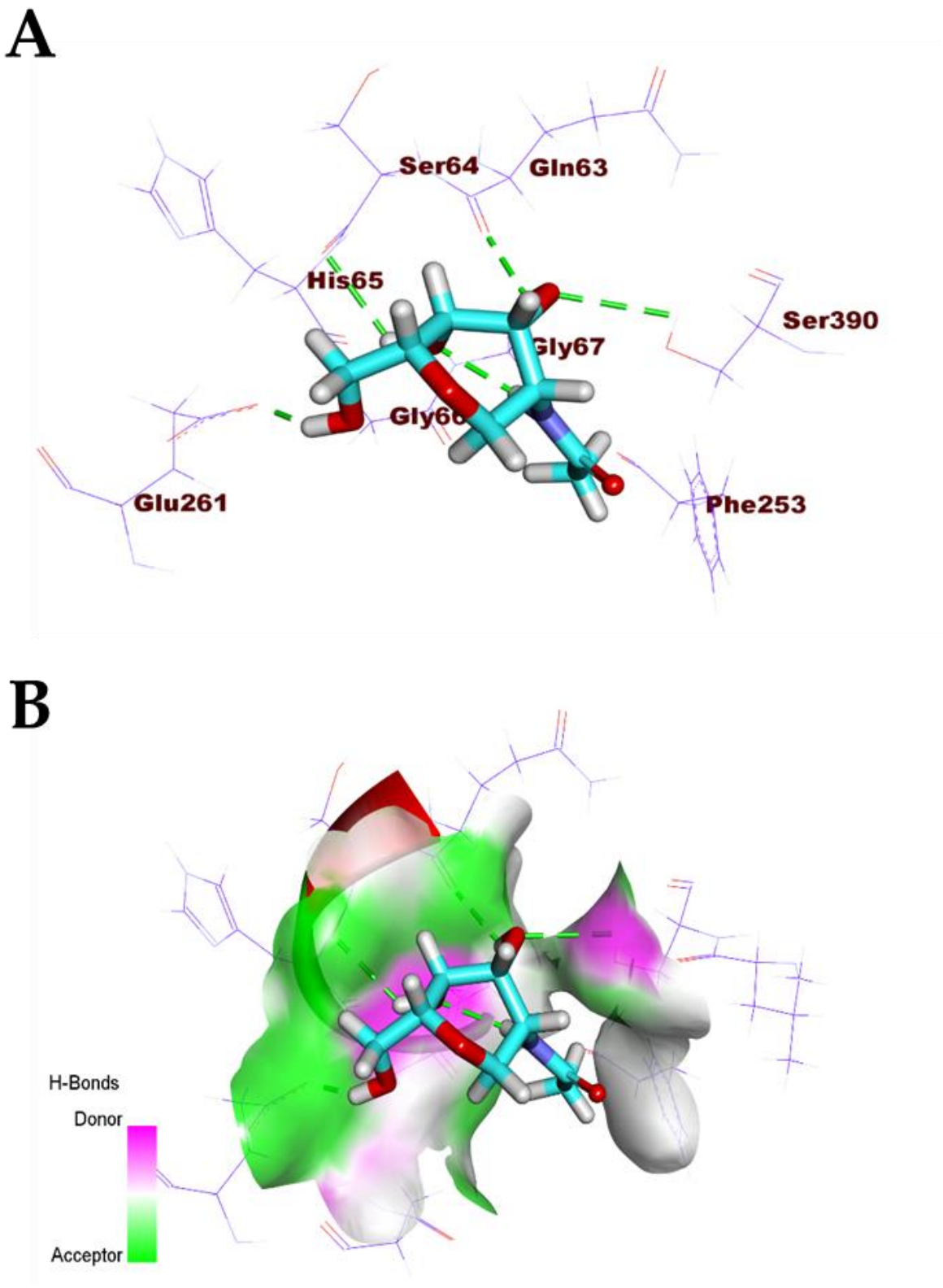

Figure 5. **A.** Co-crystallized ligand (NAG)docked into the active site of COVID-19 membrane glycoprotein. **B.** Mapping surface showing Co-crystallized ligand (NAG) occupying the active pocket of COVID-19 membrane glycoprotein.

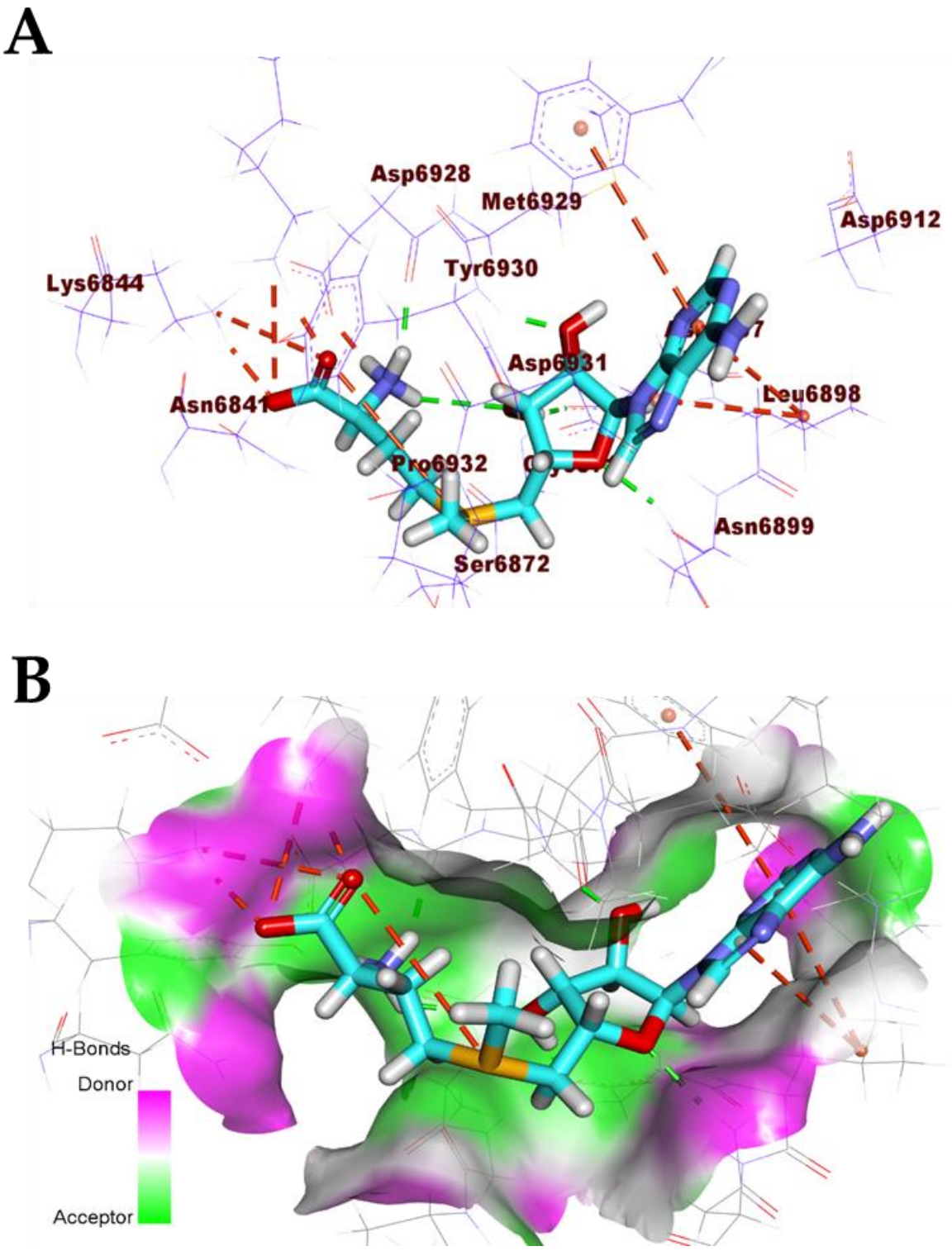

Figure 6. A. Co-crystallized ligand (SAM) docked into the active site of COVID-19 nsp10. **B.** Mapping surface showing Co-crystallized ligand (SAM) occupying the active pocket of COVID-19 nsp10.

209 The pentacyclic crambescidin 786 (**5**) exhibited a binding mode similar to that of the co-
210 crystallized ligands against COVID-19 main protease, nucleocapsid phosphoprotein, and
211 nsp10. The binding mode of compound **5** against COVID-19 main protease showed four
212 hydrogen bonds with Thr26, Ser46, and Glu166. In addition, it formed two hydrophobic
213 interactions with Lul166 and Pro168. The long ω-fatty acid chain facilitated the occupation of
214 compound **5** with different pockets of the (M^{pro}) (**Figure 7**). For the binding mode of **5** against
215 COVID-19 nucleocapsid phosphoprotein, it occupied the binding region of the target protein
216 forming one hydrogen bond with Asn75 and one hydrophobic interaction with Pro151 (**Figure**
217 **8**). Finally, the binding mode of **5** against COVID-19 nsp10 showed one hydrogen bond with
218 Asn6841 and two electrostatic interactions with Asp6912. The ω-fatty acid chain of compound
219 **5** played a vital role in the occupancy of the active site of the target protein (**Figure 9**).

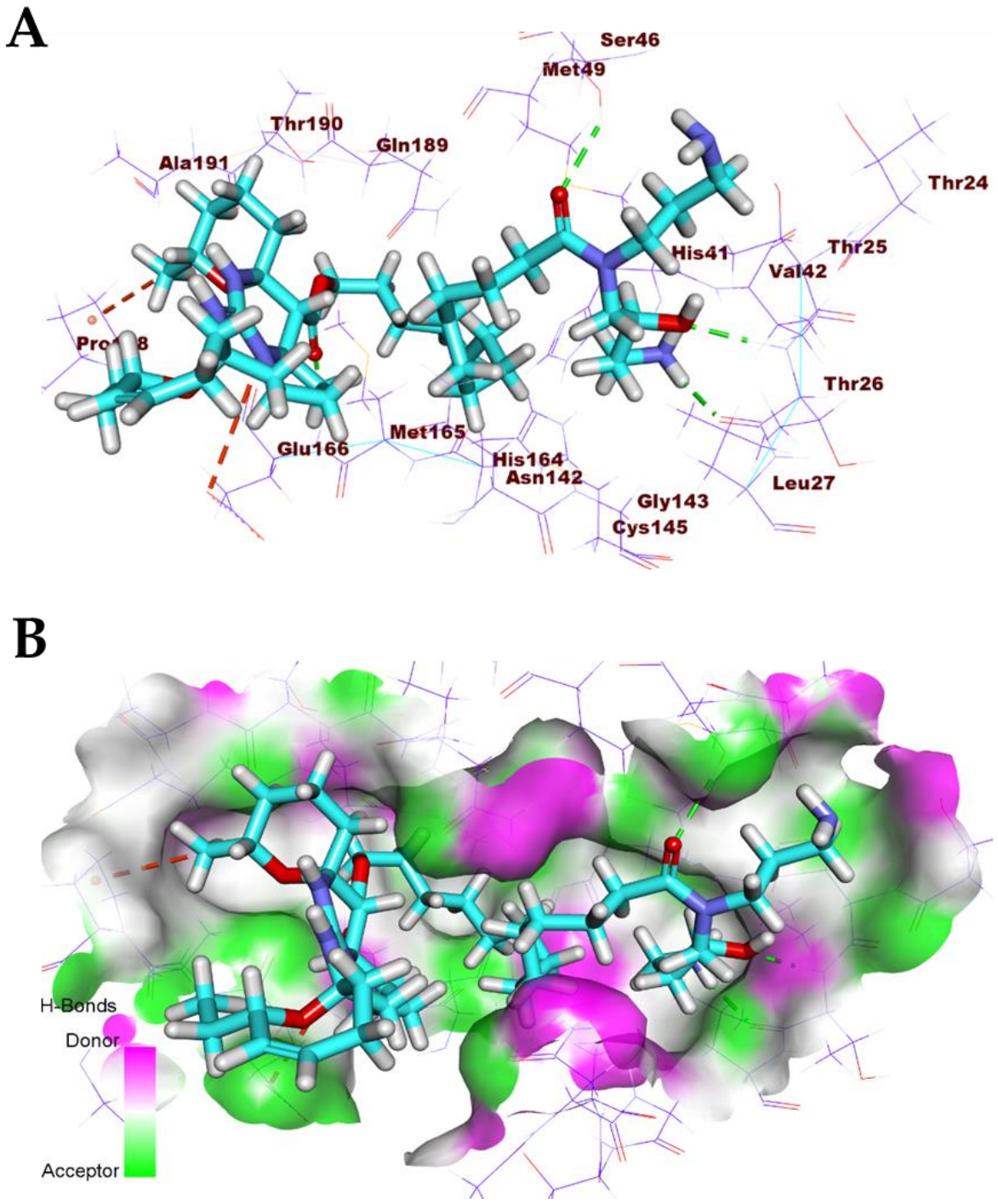

Figure 7. A. Compound 5 docked into the active site of COVID-19 main protease. **B.** Mapping surface showing Compound 5 occupying the active pocket of COVID-19 main protease.

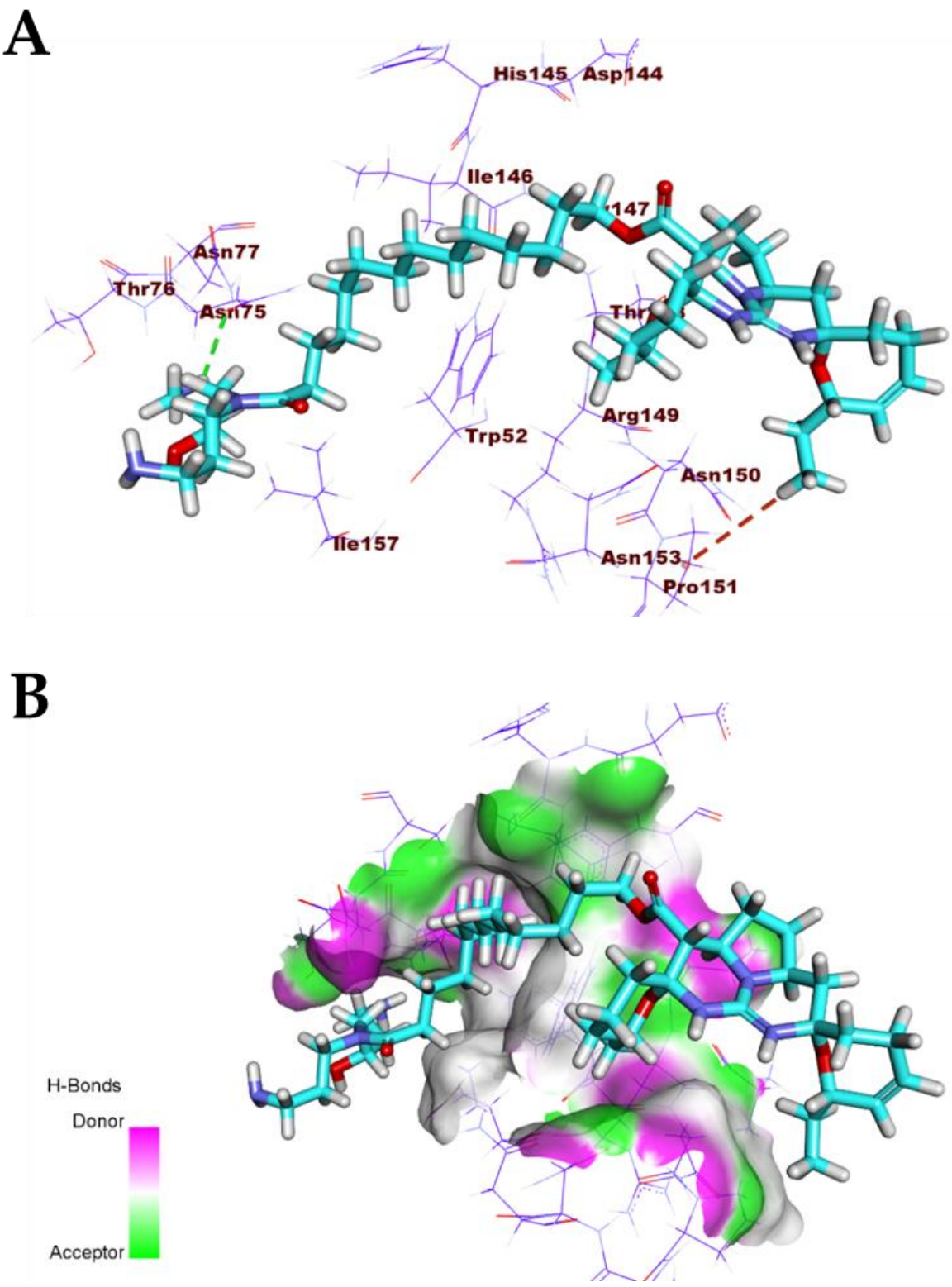

Figure 8. **A.** Compound 5 docked into the active site of COVID-19 nucleocapsid phosphoprotein. **B.** Mapping surface showing Compound 5 occupying the active pocket of COVID-19 nucleocapsid phosphoprotein.

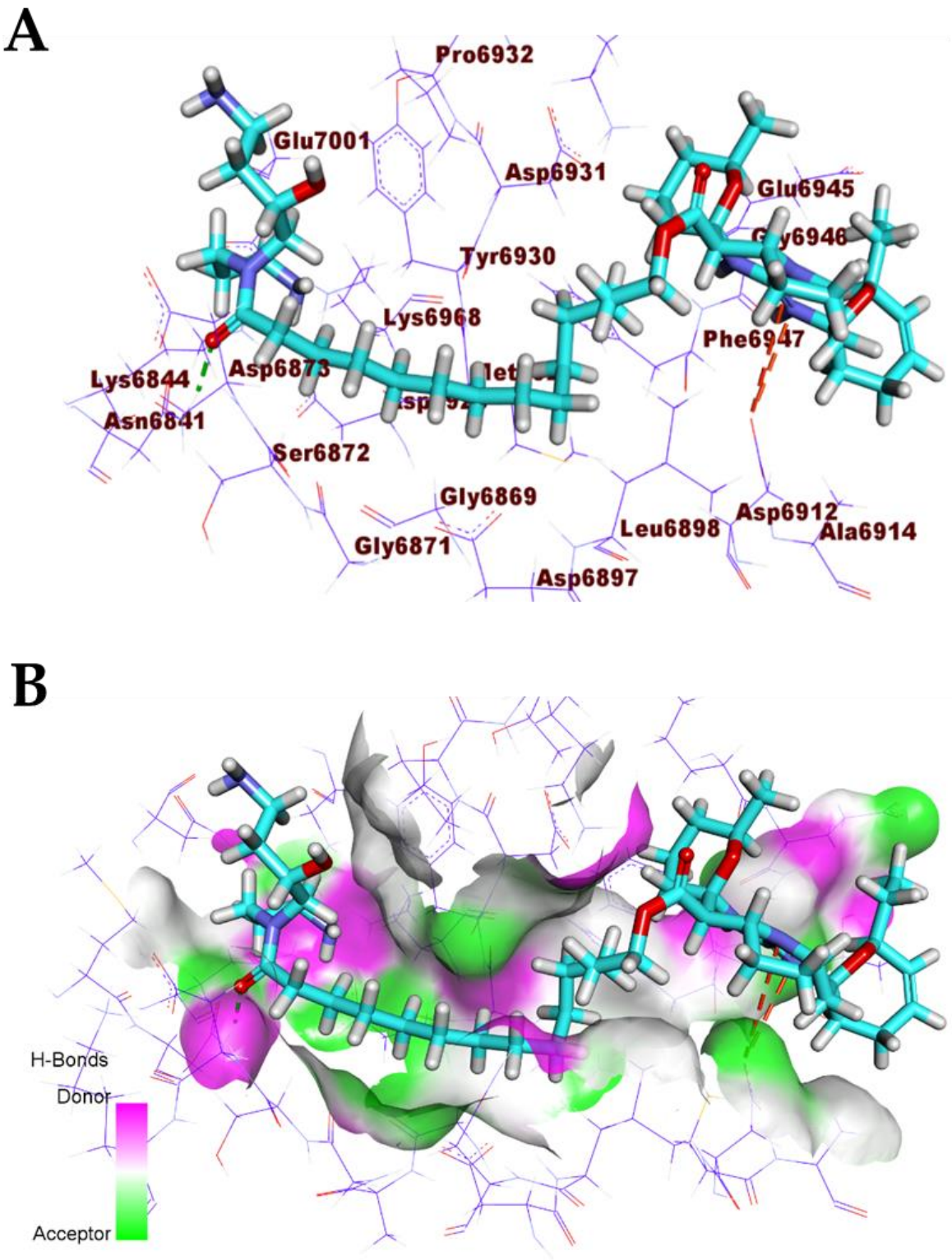

227

228 **Figure 9. A.** Compound 5 docked into the active site of COVID-19 nsp10. **B.** Mapping surface

229 showing Compound 5 occupying the active pocket of COVID-19 nsp10.

230

231

232

The pentacyclic compound, crambescidin 826 (**13)** exhibited a binding mode like that of the co-crystallized ligands against COVID-19 main protease, spike glycoproteins, and nucleocapsid phosphoprotein. The binding mode of compound **13** against COVID-19 main protease showed three hydrogen bonds with Gly143, Thr26, and Glu189. Compound **13** occupied the four pockets of the M^{pro} due to the presence of long ω-fatty acid chain (**Figure 10**). For the binding mode of compound **13** against spike glycoproteins, it formed one hydrogen bond with Tyr28 and two hydrophobic interactions with Tyr269 (**Figure 11**). Finally, the binding mode of compound **13** against COVID-19 nucleocapsid phosphoprotein showed one hydrogen bond with Thr76. In addition, it formed one hydrophobic interaction with Trp52 (**Figure 12**). On the other hand, compound **7** exhibited good affinity into the active site of COVID-19 membrane glycoprotein showing one hydrogen bond with Asp266. In addition, it formed four hydrophobic interactions with His65, Pro265, Val552, and Asp266 (**Figure 13**).

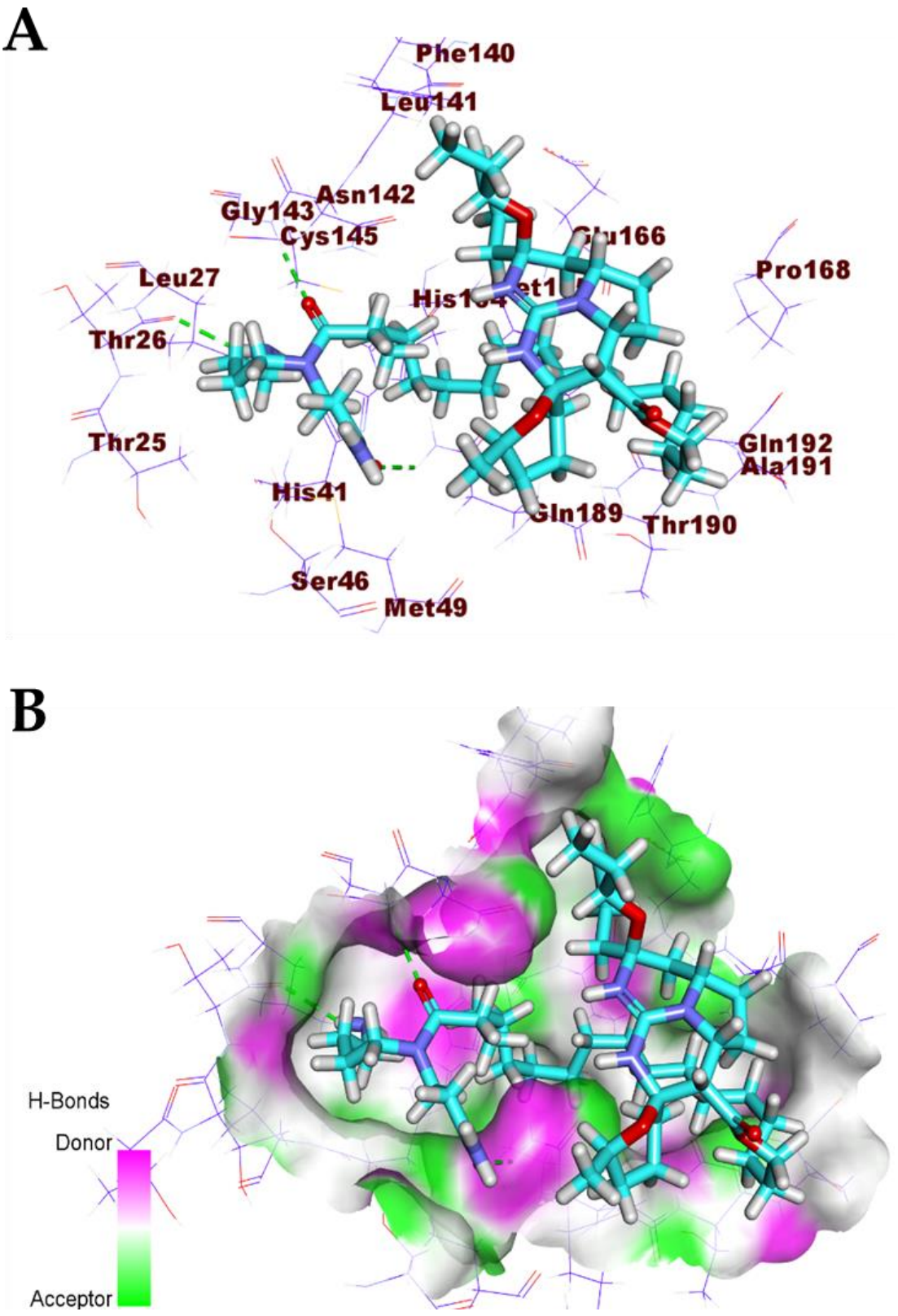

Figure 10. A. Compound 13 docked into the active site of COVID-19 main protease. **B.** Mapping surface showing Compound 13 occupying the active pocket of COVID-19 main protease.

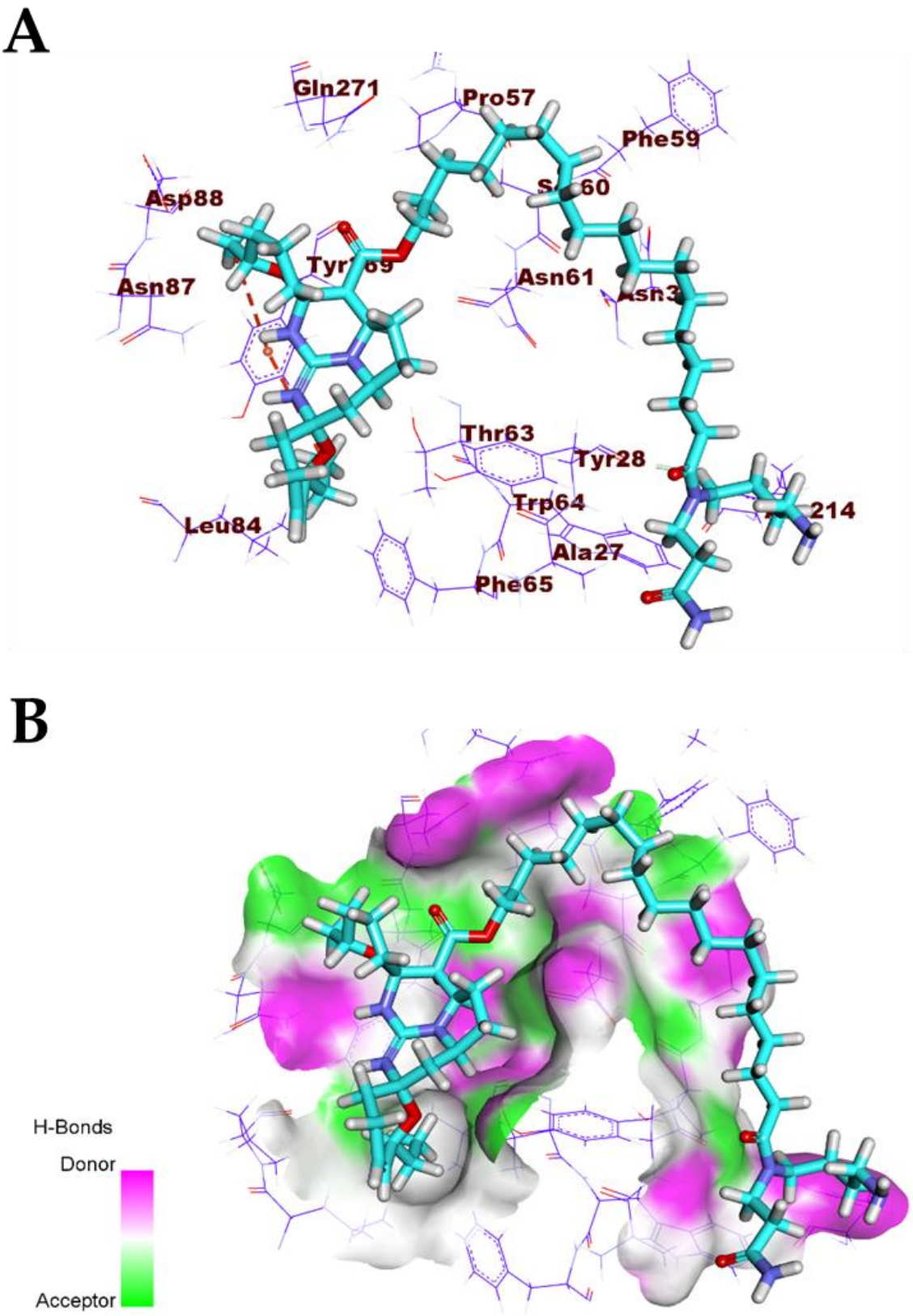

Figure 11. A. Compound 13 docked into the active site of COVID-19 spike glycoprotein. **B.** Mapping surface showing Compound 13 occupying the active pocket of COVID-19 spike glycoproteins.

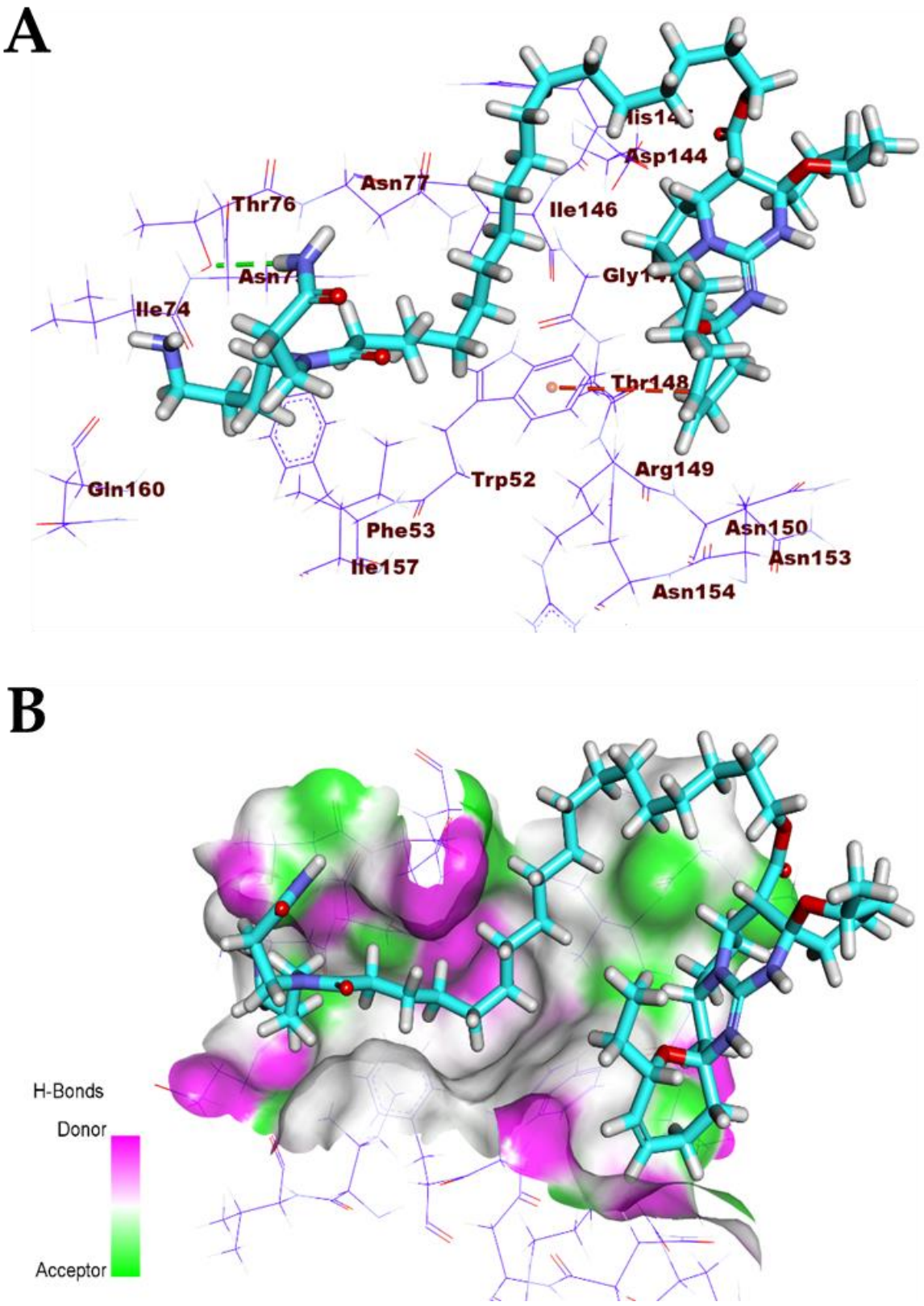

Figure 12. A. Compound 13 docked into the active site of COVID-19 nucleocapsid phosphoprotein. **B.** Mapping surface showing Compound 13 occupying the active pocket of COVID-19 Nucleocapsid phosphoprotein.

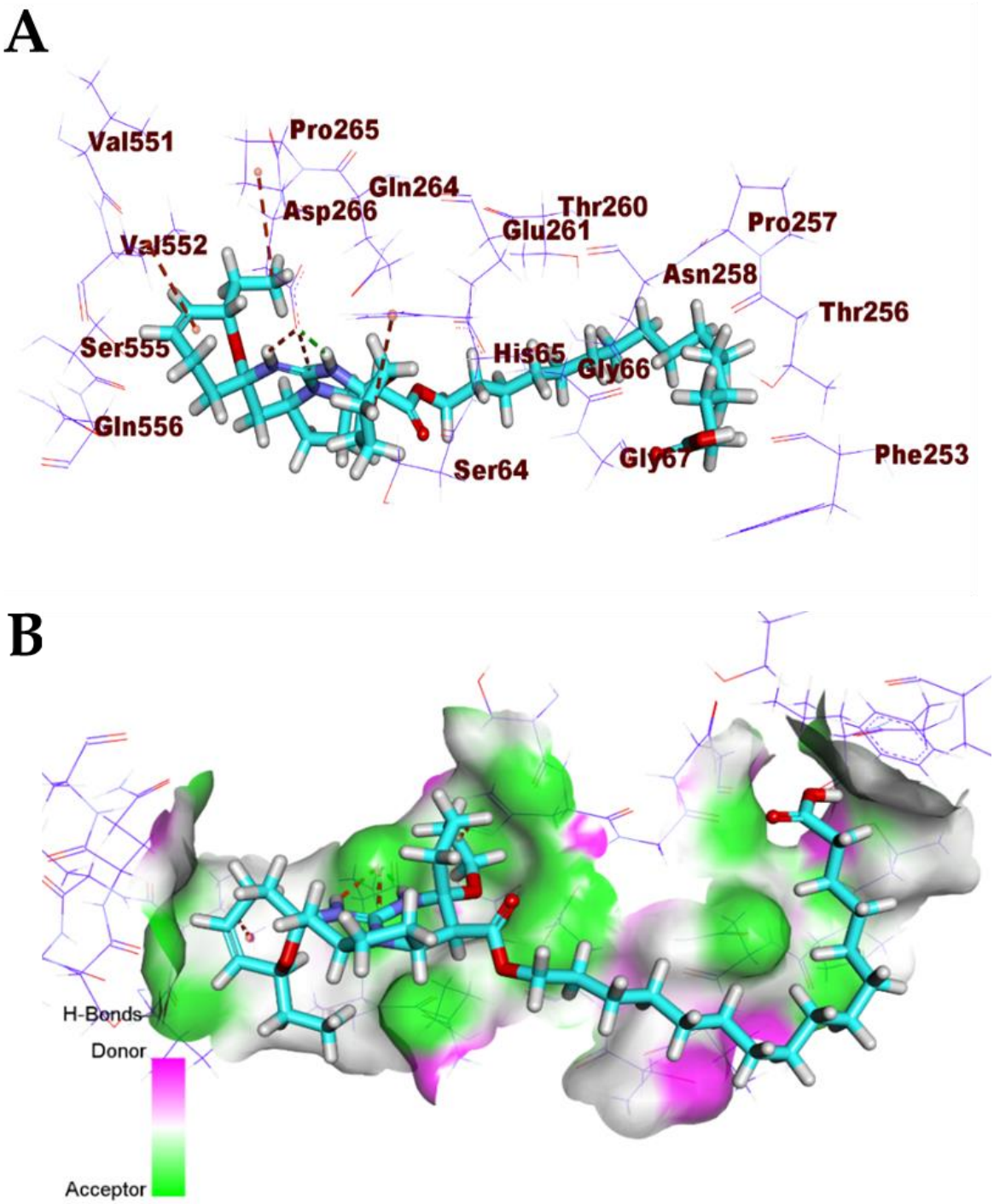

Figure 13. A. Compound 7 docked into the active site of COVID-19 membrane glycoprotein. **B.** Mapping surface showing compound 7 occupying the active pocket of COVID-19 membrane glycoprotein.

In *silico* ADMET analysis

The promising results of these docking studies enabled us to explore the ADMET characteristics and toxicity properties of the examined alkaloids. ADMET experiments can

predict different properties about these chemicals including their oral absorption, bioavailability, the ability to penetrate the blood brain barrier (BBB), their distribution, and their excretion. These properties offer valuable information about possible dose, route of administration and the safety of the examined drugs. Furthermore, these data help to reduce the risk of a compound's late stage attrition. ADMET studies were carried out for **15** guanidine alkaloids. Daclatasvir (well-studied as an antiviral) was used as a reference drug. ADMET studies include many descriptors. i) blood brain barrier penetration which predicts blood brain barrier penetration of a molecule. ii) intestinal absorption which predicts human intestinal absorption (HIA) after oral administration. iii) aqueous solubility which predicts the solubility of each compound in water at 25°C. iv) CYP2D6 binding which predicts cytochrome P450 2D6 enzyme inhibition. v) hepatotoxicity which predicts the potential hepatotoxicity of a given compound. vi) plasma protein binding which predicts the fraction of drug that while be bound by plasma proteins [72]. Discovery studio 4.0 was used to predict ADMET descriptors for all compounds. The predicted descriptors are listed in (**Table 2**). The results revealed that the tested compounds have low or very low BBB penetration levels except compounds, monalidin (**8**) and crambescidin 359 (**15**) which showed high levels of BBB penetration. Accordingly, it might be suggested that such compounds were expected to be safe to CNS. The bicyclic compounds **1**, **9** together with the pentacyclic compounds **5**-**6** and **12**-**13** showed optimal range levels of ADMET aqueous solubility. Intestinal absorption is the percentage of a drug that is absorbed across the gut wall [73]. A well-absorbed drug is one that is absorbed at least 90% into human bloodstream [74]. According to *in silico* ADMET studies, the bicyclic compounds **1**, **2**, **3**, **8**, together with the pentacyclic compound **15** were predicted to have good intestinal absorption levels, while compounds **4**, **7**, **9**, **10**, and **14** showed moderate absorption levels. The cytochrome P450 2D6 (CYP2D6) model predicts the potential of a compound to inhibit CYP2D6 enzyme using 2D chemical structure as input. CYP2D6 is an essential enzyme involved in the metabolism of a wide range of substrates in the liver. Therefore, CYP2D6 inhibition is needed as part of the regulatory procedures in the drug discovery process [75]. All examined members were predicted to be non-inhibitors of CYP2D6 except monalidin (**8**). Hepatotoxicity prediction of such compounds revealed that all compounds are non-hepatotoxic except the bicyclic compound monalidin (**8**). Consequently, liver dysfunction side effect is not expected upon administration of these compounds. The plasma protein binding

296 model predicts whether a compound is likely to be highly bound (>= 90% bound) to carrier
297 proteins in the blood [76]. All compounds were expected to bind plasma protein less than 90%
298 except compound **8** (**Figure 14**)

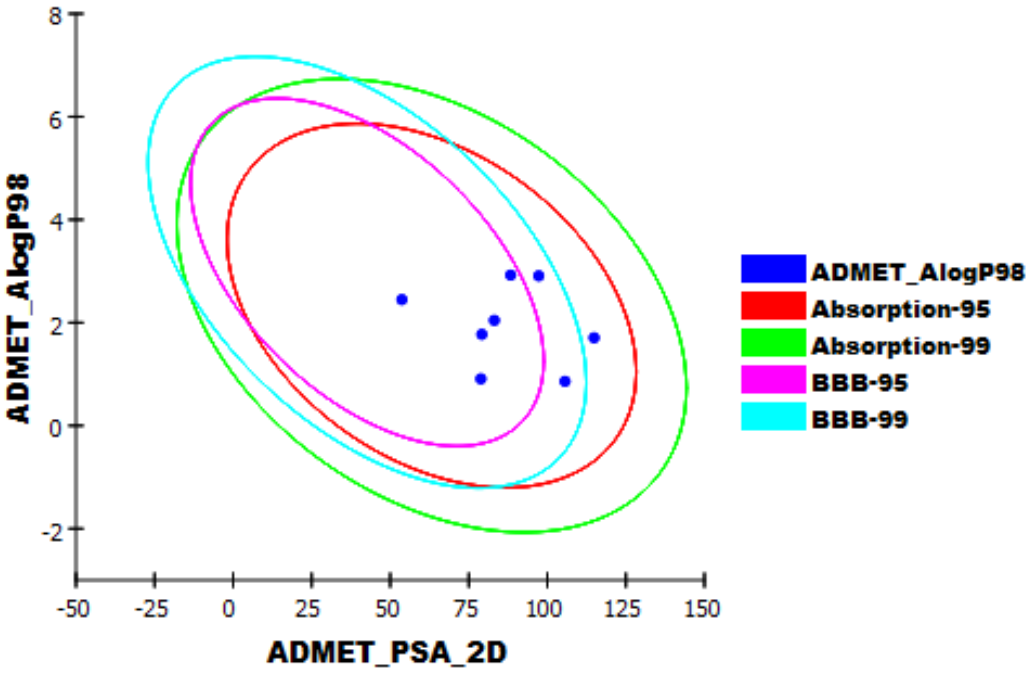

299

300 **Figure 14.** The expected ADMET study.

301

302 **Table 2.** Predicted ADMET for 15 guanidine alkaloids and reference drug, Daclatasvir.

Compounds	BBB level [a]	Solubility level [b]	Absorption level [c]	CYP2D6 prediction [d]	Hepatotoxicity prediction [e]	PPB prediction [f]
Monanchoradin A (**1**)	3	4	0	FALSE	FALSE	FALSE
Monanchoradin B (**2**)	3	3	0	FALSE	FALSE	FALSE
Monanchoradin C (**3**)	3	3	0	FALSE	FALSE	FALSE
Dehydrocrambescin A2 418 **(4)**	4	3	2	FALSE	FALSE	FALSE
Crambescidin 786 (**5**)	4	4	3	FALSE	FALSE	FALSE
Crambescidin 814 (**6**)	4	4	3	FALSE	FALSE	FALSE
Norcrambescidic acid (**7**)	4	2	2	FALSE	FALSE	FALSE
Monalidin (**8**)	1	2	0	TRUE	TRUE	TRUE
(-)-crambescin A2 392 (**9**)	4	4	1	FALSE	FALSE	FALSE
(-)-crambescin A2 406 (**10**)	4	3	1	FALSE	FALSE	FALSE
(-)-crambescin A2 420 (**11**)	4	3	2	FALSE	FALSE	FALSE

Crambescidin 800 (**12**)	4	4	3	FALSE	FALSE	FALSE
Crambescidin 826 (**13**)	4	4	3	FALSE	FALSE	FALSE
Crambescidic acid (**14**)	4	2	2	FALSE	FALSE	FALSE
Crambescidin 359 (**15**)	1	2	0	FALSE	FALSE	FALSE
Daclatasvir	4	3	3	FALSE	TRUE	TRUE

[a] BBB level, blood brain barrier level, 0 = very high, 1 = high, 2 = medium, 3 = low, 4 = very low.

[b] Solubility level, 1 = very low, 2 = low, 3 = good, 4 = optimal.

[c] Absorption level, 0 = good, 1 = moderate, 2 = poor, 3 = very poor.

[d] CYP2D6, cytochrome P2D6, TRUE = inhibitor, FALSE = non inhibitor.

[e] Hepatotoxicity, TRUE = hepatotoxic, FALSE = non-hepatotoxic.

[f] PBB, plasma protein binding, FALSE means less than 90%, TRUE means more than 90%

Toxicity studies

A toxicity prediction was carried out for the 15 guanidine alkaloids based on validated models in Discovery studio software [77, 78] as follows: i) FDA rodent carcinogenicity which computes the probability of a chemical being a carcinogen. ii) carcinogenic potency TD50 which predicts the tumorigenic dose rate 50 (TD50) of a chemical in a rodent chronic exposure toxicity test [79]. iii) rat maximum tolerated dose which predicts the rat maximum tolerated dose (MTD) of a chemical [80, 81]. iv) rat oral LD50 which predicts the rat oral acute median lethal dose (LD50) in the toxicity test of a chemical [82]. v) rat chronic LOAEL which predicts the rat chronic lowest observed adverse effect level (LOAEL) value of a chemical [83, 84]. As shown in **Table 3**, the tested compounds showed *in silico* expected low toxicity against the tested models. For the FDA rodent carcinogenicity model, the tested compounds were expected to be non-carcinogenic. For the carcinogenic potency TD50 mouse model, all compounds showed TD50 values higher than that of the reference drug Daclatasvir. Regarding the rat maximum tolerated dose model, the compounds showed maximum tolerated doses with a range of 0.027 to 0.350 g/kg body weight, which are all higher than Daclatasvir **(**0.022 g/kg body weight). For the rat oral LD50 model, compounds **4**-**15** showed oral LD50 values ranging from 1.829 to 13.415 mg/kg body weight/day. These values are higher than that of Daclatasvir **(**0.677 mg/kg body weight/day). For the rat chronic LOAEL model, compounds **1-4** and **8-11** showed LOAEL values ranging from 0.0165 to 0.0450 g/kg body weight. These values are similar or higher than that of

329 Daclatasvir (0.0063 g/kg body weight). Compounds **5**-**7** and **12**-**15** showed LOAEL values of
330 ranging from 0.0012 to 0.0019 g/kg body weight, which is less than Daclatasvir.

331 **Table 3:** Toxicity properties of the most promising compounds (**1-15**)

Compounds	FDA Rodent Carcinogenicity	Carcinogenic potency TD_{50} mouse [a]	Rat Maximum Tolerated Dose (Feed) [b]	Rat Oral LD_{50} [b]	Rat Chronic LOAEL [b]
Monanchoradin A (**1**)	Non-Carcinogen	51.0661	0.085	0.399	0.0168
Monanchoradin B (**2**)	Non-Carcinogen	52.712	0.091	0.457	0.0167
Monanchoradin C (**3**)	Non-Carcinogen	54.2866	0.098	0.509	0.0166
Dehydrocrambescin A2 418 **(4)**	Non-Carcinogen	19.5925	0.573	10.139	0.0450
Crambescidin 786 (**5**)	Non-Carcinogen	1.91771	0.063	10.559	0.0019
Crambescidin 814 (**6**)	Non-Carcinogen	1.91977	0.071	13.415	0.0017
Norcrambescidic acid (**7**)	Non-Carcinogen	5.77105	0.043	11.836	0.0013
Monalidin (**8**)	Non-Carcinogen	32.2161	0.123	3.156	0.0448
(-)-crambescin A2 392 (**9**)	Non-Carcinogen	39.9613	0.310	2.634	0.0171
(-)-crambescin A2 406 (**10)**	Non-Carcinogen	40.6645	0.329	2.970	0.0168
(-)-crambescin A2 420 (**11)**	Non-Carcinogen	41.3406	0.350	3.269	0.0165
Crambescidin 800 (**12**)	Non-Carcinogen	1.91899	0.065	11.440	0.0018
Crambescidin 826 (**13**)	Non-Carcinogen	1.30045	0.042	14.200	0.0012
Crambescidic acid (**14**)	Non-Carcinogen	5.07065	0.040	8.153	0.0018
Crambescidin 359 (**15**)	Non-Carcinogen	0.779067	0.027	1.829	0.0021
Daclatasvir	Non-Carcinogen	0.970599	0.022	0.677	0.0063

332 [a] mg/kg body weight/day, [b] Unit: g/kg body weight

333

334

335

CONCLUSIONS

Fifteen structurally divergent polycyclic guanidine alkaloids were comprehensively investigated for their virtual antiviral potentials against five SARS-Cov-2 (Covid-19) proteins. The pentacyclic guanidinic scaffolds, crambescidins 786 (5) and 826 (13) displayed the best docking results among the 15 investigated compounds. The examined compounds exhibited very well *in silico* ADMET results and showed no toxicity. Such computational results highlight the polycyclic guanidinic marine alkaloids as robust and promising antiviral molecular architectures, which worth further experimental and theoretical investigations.

EXPERIMENTAL SECTION

Docking studies

The crystal structures of the target proteins: i) COVID-19 main protease (M^{pro}) (PDB ID: 6lu7, resolution: 2.16 Å), ii) spike glycoproteins (PDB ID: 6VYB, resolution: 3.20 Å), iii) nucleocapsid phosphoprotein (PDB ID: 6VYO, resolution: 1.70 Å), iv) membrane glycoprotein (PDB ID: 6M17, resolution: 2.90 Å), and v) nsp10 (PDB ID: 6W4H, resolution: 1.80 Å) were downloaded from Protein Data Bank (http://www.pdb.org). Molecular Operating Environment (MOE) was used for the docking analysis [85]. In these studies, the free energies and binding modes of the examined molecules against target proteins were determined. At first, the water molecules were removed from the crystal structures of target proteins, retaining only main chain amino acids which are essential for binding. The Co-crystallized ligands were used as reference ligands. Then, the protein structures were protonated, and the hydrogen atoms were hidden. Next, the energy was minimized and the binding pockets of each protein was defined [86, 87]. The structures of the examined compounds and the co-crystallized ligands were drawn using ChemBioDraw Ultra 14.0 and saved using SDF formats. Then, the saved files were opened using MOE software and 3D structures were protonated. Next, the energy of the molecules was minimized. Validation processes were performed for each target receptor by running the docking process for only the co-crystallized ligand. Low RMSD values between docked and crystal conformations indicated valid performances [88, 89]. The docking procedures were carried out utilizing a default protocol. In each case, 10 docked structures were generated using genetic algorithm searches. The output

from MOE software was further analyzed and visualized using Discovery Studio 4.0 software [89-92].

ADMET

ADMET descriptors (absorption, distribution, metabolism, excretion and toxicity) of the compounds were determined using Discovery studio 4.0. Initially, the CHARMM force field was applied then the compounds were prepared and minimized according to the preparation for small molecules protocol. Then ADMET descriptors protocol was applied to carry out these studies [88, 91].

Toxicity

The toxicity parameters were calculated using Discovery studio 4.0. Daclatasvir was used as a reference drug. Initially, CHARMM force field was applied then the compounds were prepared and minimized according to the preparation for small molecules protocol. Then different parameters were calculated using toxicity prediction (extensible) protocols.

Isolation and characterization of compounds 1-15

Compounds **1-15** were isolated and identified from the French Polynesian marine sponge, Monanchora n. sp. For detailed isolation and structural characterizations, see El-Demerdash. *et al*., [45].

AUTHOR INFORMATION

Corresponding Author

*E-mails: (A.E.-D) eldemerdash555@gmail.com; (A.M.M) ametwaly@azhar.edu.eg; (J.D.S.) stockand@uthscsa.edu.

Author Contributions

Conceptualization, A.E.-D., A.M.M. and I.H.E.; methodology, A.M.M. and I.H.E.; software, A.M.M. and I.H.E.; writing-original draft preparation, A.E.-D., A.M.M., T.M.A. and I.H.E.; writing-review and editing, A.E.-D., A.M.M., T.M.A., I.H.E. and J.D.S.; supervision, A.E.-D., A.M.M. and J.D.S. All authors have read and agreed to the published version of the manuscript.

Notes

The authors declare no competing financial interest.

ACKNOWLEDGMENTS

Financial support from CNRS-ICSN and ANR (POMARE project, 2011-EBIM-006-01) are gratefully acknowledged. A.E.-D.'s Ph.D. was granted and financed by the Egyptian Government (Ministry of Higher Education), they are gratefully acknowledged.

ABBREVIATIONS USED

ADMET, Absorption, Distribution, Metabolism, Excretion, and Toxicity; FDA, Food and Drug Administration; TD_{50}, Median Toxic Dose; LD_{50}, Median Lethal Dose; LOAEL, Lowest Observed Adverse Effect Level; MNPs, Marine Natural Products; PGAs, Polycyclic Guanidine Alkaloids; HIV-1, Human Immunodeficiency Virus; MOE, Molecular Operating Environment

REFERENCES

1. Abd El-Aziz, T. M.; Stockand, J. D. Recent progress and challenges in drug development against COVID-19 coronavirus (SARS-CoV-2) - an update on the status. *Infect Genet Evol* **2020,** 83, 104327-104327.

2. Steffens, I. A hundred days into the coronavirus disease (COVID-19) pandemic. *Euro surveillance : bulletin Europeen sur les maladies transmissibles = European communicable disease bulletin* **2020,** 25, 2000550.

3. Fehr, A. R.; Perlman, S. Coronaviruses: an overview of their replication and pathogenesis. *Methods Mol Biol* **2015,** 1282, 1-23.

4. Weiss, S. R.; Navas-Martin, S. Coronavirus pathogenesis and the emerging pathogen severe acute respiratory syndrome coronavirus. *Microbiology and molecular biology reviews : MMBR* **2005,** 69, 635-64.

5. Bradburne, A. F.; Tyrrell, D. A. The propagation of "coronaviruses" in tissue-culture. *Archiv fur die gesamte Virusforschung* **1969,** 28, 133-50.

6. Zumla, A.; Chan, J. F.; Azhar, E. I.; Hui, D. S.; Yuen, K. Y. Coronaviruses - drug discovery and therapeutic options. *Nature reviews. Drug discovery* **2016,** 15, 327-47.

7. Su, S.; Wong, G.; Shi, W.; Liu, J.; Lai, A. C. K.; Zhou, J.; Liu, W.; Bi, Y.; Gao, G. F. Epidemiology, Genetic Recombination, and Pathogenesis of Coronaviruses. *Trends in microbiology* **2016,** 24, 490-502.

8. Forni, D.; Cagliani, R.; Clerici, M.; Sironi, M. Molecular Evolution of Human Coronavirus Genomes. *Trends in microbiology* **2017,** 25, 35-48.

9. Huang, X.; Dong, W.; Milewska, A.; Golda, A.; Qi, Y.; Zhu, Q. K.; Marasco, W. A.; Baric, R. S.; Sims, A. C.; Pyrc, K.; Li, W.; Sui, J. Human Coronavirus HKU1 Spike Protein Uses O-Acetylated Sialic Acid as an Attachment Receptor Determinant and Employs Hemagglutinin-Esterase Protein as a Receptor-Destroying Enzyme. *J Virol* **2015,** 89, 7202-13.

10. Ge, X. Y.; Li, J. L.; Yang, X. L.; Chmura, A. A.; Zhu, G.; Epstein, J. H.; Mazet, J. K.; Hu, B.; Zhang, W.; Peng, C.; Zhang, Y. J.; Luo, C. M.; Tan, B.; Wang, N.; Zhu, Y.; Crameri, G.; Zhang, S. Y.; Wang, L. F.; Daszak, P.; Shi, Z. L. Isolation and characterization of a bat SARS-like coronavirus that uses the ACE2 receptor. *Nature* **2013,** 503, 535-8.

11. de Wit, E.; van Doremalen, N.; Falzarano, D.; Munster, V. J. SARS and MERS: recent insights into emerging coronaviruses. *Nature reviews. Microbiology* **2016,** 14, 523-34.

12. Ithete, N. L.; Stoffberg, S.; Corman, V. M.; Cottontail, V. M.; Richards, L. R.; Schoeman, M. C.; Drosten, C.; Drexler, J. F.; Preiser, W. Close relative of human Middle East respiratory syndrome coronavirus in bat, South Africa. *Emerg Infect Dis* **2013,** 19, 1697-1699.

13. Patiño-Galindo, J. Á.; Filip, I.; AlQuraishi, M.; Rabadan, R. Recombination and convergent evolution led to the emergence of 2019 Wuhan coronavirus. *bioRxiv* **2020**, 2020.02.10.942748.

14. Zhou, P.; Yang, X. L.; Wang, X. G.; Hu, B.; Zhang, L.; Zhang, W.; Si, H. R.; Zhu, Y.; Li, B.; Huang, C. L.; Chen, H. D.; Chen, J.; Luo, Y.; Guo, H.; Jiang, R. D.; Liu, M. Q.; Chen, Y.; Shen, X. R.; Wang, X.; Zheng, X. S.; Zhao, K.; Chen, Q. J.; Deng, F.; Liu, L. L.; Yan, B.; Zhan, F. X.; Wang, Y. Y.; Xiao, G. F.; Shi, Z. L. A pneumonia outbreak associated with a new coronavirus of probable bat origin. *Nature* **2020,** 579, 270-273.

15. Ren, L. L.; Wang, Y. M.; Wu, Z. Q.; Xiang, Z. C.; Guo, L.; Xu, T.; Jiang, Y. Z.; Xiong, Y.; Li, Y. J.; Li, X. W.; Li, H.; Fan, G. H.; Gu, X. Y.; Xiao, Y.; Gao, H.; Xu, J. Y.; Yang, F.; Wang, X. M.; Wu, C.; Chen, L.; Liu, Y. W.; Liu, B.; Yang, J.; Wang, X. R.; Dong, J.; Li, L.; Huang, C. L.; Zhao, J. P.; Hu, Y.; Cheng, Z. S.; Liu, L. L.; Qian, Z. H.; Qin, C.; Jin, Q.; Cao, B.; Wang, J. W. Identification of a novel coronavirus causing severe pneumonia in human: a descriptive study. *Chinese medical journal* **2020,** 133, 1015-1024.

16. Rossmann, M. G. Structure of viruses: a short history. *Quarterly reviews of biophysics* **2013,** 46, 133.

17. Lodish, H.; Berk, A.; Zipursky, S. L.; Matsudaira, P.; Baltimore, D.; Darnell, J. Viruses: Structure, function, and uses. In *Molecular Cell Biology. 4th edition*, WH Freeman: 2000.

18. Pornillos, O.; Garrus, J. E.; Sundquist, W. I. Mechanisms of enveloped RNA virus budding. *Trends in cell biology* **2002,** 12, 569-579.

19. Li, X.; Geng, M.; Peng, Y.; Meng, L.; Lu, S. Molecular immune pathogenesis and diagnosis of COVID-19. *Journal of Pharmaceutical Analysis* **2020**.

20. Zhang, L.; Lin, D.; Sun, X.; Curth, U.; Drosten, C.; Sauerhering, L.; Becker, S.; Rox, K.; Hilgenfeld, R. Crystal structure of SARS-CoV-2 main protease provides a basis for design of improved α-ketoamide inhibitors. *Science* **2020,** 368, 409-412.

21. Prajapat, M.; Sarma, P.; Shekhar, N.; Avti, P.; Sinha, S.; Kaur, H.; Kumar, S.; Bhattacharyya, A.; Kumar, H.; Bansal, S. Drug targets for corona virus: A systematic review. *Indian journal of pharmacology* **2020,** 52, 56.

22. Bouvet, M.; Lugari, A.; Posthuma, C. C.; Zevenhoven, J. C.; Bernard, S.; Betzi, S.; Imbert, I.; Canard, B.; Guillemot, J.-C.; Lécine, P. Coronavirus Nsp10, a critical co-factor for activation of multiple replicative enzymes. *Journal of Biological Chemistry* **2014,** 289, 25783-25796.

23. Bergmann, W.; Burke, D. C. CONTRIBUTIONS TO THE STUDY OF MARINE PRODUCTS. XXXIX. THE NUCLEOSIDES OF SPONGES. III.1 SPONGOTHYMIDINE AND SPONGOURIDINE2. *The Journal of Organic Chemistry* **1955,** 20, 1501-1507.

24. Newman, D. J.; Cragg, G. M. Natural Products as Sources of New Drugs from 1981 to 2014. *J. Nat. Prod.* **2016,** 79, 629-661.

25. Dias, D. A.; Urban, S.; Roessner, U. A Historical Overview of Natural Products in Drug Discovery. *Metabolites* **2012,** 2, 303-336.

26. Mayer, A. M. S.; Glaser, K. B.; Cuevas, C.; Jacobs, R. S.; Kem, W.; Little, R. D.; McIntosh, J. M.; Newman, D. J.; Potts, B. C.; Shuster, D. E. The odyssey of marine pharmaceuticals: a current pipeline perspective. *Trends Pharmacol. Sci.* **2010,** 31, 255-265.

27. Montaser, R.; Luesch, H. Marine natural products: a new wave of drugs? *Future Medicinal Chemistry* **2011,** 3, 1475-1489.

28. Altmann, K.-H. Drugs from the Oceans: Marine Natural Products as Leads for Drug Discovery. *CHIMIA International Journal for Chemistry* **2017,** 71, 646-652.

29. Jiménez, C. Marine Natural Products in Medicinal Chemistry. *ACS Medicinal Chemistry Letters* **2018,** 9, 959-961.

30. Pereira, F. Have marine natural product drug discovery efforts been productive and how can we improve their efficiency? *Expert Opinion on Drug Discovery* **2019,** 14, 717-722.

31. Donia, M.; Hamann, M. T. Marine natural products and their potential applications as anti-infective agents. *The Lancet Infectious Diseases* **2003,** 3, 338-348.

32. Williams, D. E.; Andersen, R. J. Biologically active marine natural products and their molecular targets discovered using a chemical genetics approach. *Natural Product Reports* **2020,** 37, 617-633.

33. Álvarez-Bardón, M.; Pérez-Pertejo, Y.; Ordóñez, C.; Sepúlveda-Crespo, D.; Carballeira, N. M.; Tekwani, B. L.; Murugesan, S.; Martinez-Valladares, M.; García-Estrada, C.; Reguera, R. M.; Balaña-Fouce, R. Screening Marine Natural Products for New Drug Leads against Trypanosomatids and Malaria. *Mar. Drugs* **2020,** 18, 187.

34. Khan, M. T.; Ali, A.; Wang, Q.; Irfan, M.; Khan, A.; Zeb, M. T.; Zhang, Y.-J.; Chinnasamy, S.; Wei, D.-Q. Marine natural compounds as potents inhibitors against the main protease of SARS-CoV-2—a molecular dynamic study. *J. Biomol. Struct. Dyn.* **2020**, 1-11.

35. Carroll, A. R.; Copp, B. R.; Davis, R. A.; Keyzers, R. A.; Prinsep, M. R. Marine natural products. *Natural Product Reports* **2020,** 37, 175-223.

36. Yasuhara-Bell, J.; Lu, Y. Marine compounds and their antiviral activities. *Antiviral Res.* **2010,** 86, 231-240.

37. Gogineni, V.; Schinazi, R. F.; Hamann, M. T. Role of Marine Natural Products in the Genesis of Antiviral Agents. *Chem. Rev.* **2015,** 115, 9655-9706.

38. El-Demerdash, A.; Atanasov, A. G.; Bishayee, A.; Abdel-Mogib, M.; Hooper, J. N. A.; Al-Mourabit, A. Batzella, Crambe and Monanchora: Highly Prolific Marine Sponge Genera Yielding Compounds with Potential Applications for Cancer and Other Therapeutic Areas. *Nutrients* **2018,** 10, 33.

39. Sfecci, E.; Lacour, T.; Amade, P.; Mehiri, M. Polycyclic Guanidine Alkaloids from Poecilosclerida Marine Sponges. *Mar. Drugs* **2016,** 14, 77.

504 40. El-Demerdash, A.; Tammam, M. A.; Atanasov, A. G.; Hooper, J. N. A.; Al-Mourabit, A.; Kijjoa, A.
505 Chemistry and Biological Activities of the Marine Sponges of the Genera Mycale (Arenochalina),
506 Biemna and Clathria. *Mar. Drugs* **2018,** 16, 214.
507 41. Kashman, Y.; Hirsh, S.; McConnell, O. J.; Ohtani, I.; Kusumi, T.; Kakisawa, H. Ptilomycalin A: a
508 novel polycyclic guanidine alkaloid of marine origin. *J. Am. Chem. Soc.* **1989,** 111, 8925-8926.
509 42. El-Demerdash, A.; Ermolenko, L.; Gros, E.; Retailleau, P.; Thanh, B. N.; Anne, G.-B.; Al-Mourabit,
510 A. Short-Cut Bio-Inspired Synthesis of Tricyclic Guanidinic Motifs of Crambescidins and Batzelladines
511 Marine Alkaloids. *Eur. J. Org. Chem.* n/a.
512 43. Jares-Erijman, E. A.; Sakai, R.; Rinehart, K. L. Crambescidins: new antiviral and cytotoxic
513 compounds from the sponge Crambe crambe. *The Journal of Organic Chemistry* **1991,** 56, 5712-5715.
514 44. Rubiolo, J. A.; López-Alonso, H.; Roel, M.; Vieytes, M. R.; Thomas, O.; Ternon, E.; Vega, F. V.;
515 Botana, L. M. Mechanism of cytotoxic action of crambescidin-816 on human liver-derived tumour cells.
516 *Br. J. Pharmacol.* **2014,** 171, 1655-1667.
517 45. El-Demerdash, A.; Moriou, C.; Martin, M.-T.; Rodrigues-Stien, A. d. S.; Petek, S.; Demoy-
518 Schneider, M.; Hall, K.; Hooper, J. N. A.; Debitus, C.; Al-Mourabit, A. Cytotoxic Guanidine Alkaloids
519 from a French Polynesian Monanchora n. sp. Sponge. *J. Nat. Prod.* **2016,** 79, 1929-1937.
520 46. El-Demerdash, A.; Moriou, C.; Martin, M.-T.; Petek, S.; Debitus, C.; Al-Mourabit, A. Unguiculins
521 A-C: cytotoxic bis-guanidine alkaloids from the French Polynesian sponge, Monanchora n. sp. *Nat.*
522 *Prod. Res.* **2018,** 32, 1512-1517.
523 47. Mendez, A. G.; Juncal, A. B.; Silva, S. B. L.; Thomas, O. P.; Martín Vázquez, V.; Alfonso, A.; Vieytes,
524 M. R.; Vale, C.; Botana, L. M. The Marine Guanidine Alkaloid Crambescidin 816 Induces Calcium Influx
525 and Cytotoxicity in Primary Cultures of Cortical Neurons through Glutamate Receptors. *ACS Chemical*
526 *Neuroscience* **2017,** 8, 1609-1617.
527 48. Shrestha, S.; Sorolla, A.; Fromont, J.; Blancafort, P.; Flematti, G. R. Crambescidin 800, Isolated from
528 the Marine Sponge Monanchora viridis, Induces Cell Cycle Arrest and Apoptosis in Triple-Negative
529 Breast Cancer Cells. *Mar. Drugs* **2018,** 16, 53.

530 49. Shubina, L. K.; Makarieva, T. N.; von Amsberg, G.; Denisenko, V. A.; Popov, R. S.; Dyshlovoy, S.
531 A. Monanchoxymycalin C with anticancer properties, new analogue of crambescidin 800 from the
532 marine sponge Monanchora pulchra. *Nat. Prod. Res.* **2019,** 33, 1415-1422.
533 50. Palagiano, E.; De Marino, S.; Minale, L.; Riccio, R.; Zollo, F.; Iorizzi, M.; Carré, J. B.; Debitus, C.;
534 Lucarain, L.; Provost, J. Ptilomycalin A, crambescidin 800 and related new highly cytotoxic guanidine
535 alkaloids from the starfishes Fromia monilis and Celerina heffernani. *Tetrahedron* **1995,** 51, 3675-3682.
536 51. Amade, P.; Charroin, C.; Baby, C.; Vacelet, J. Antimicrobial activities of marine sponges from the
537 Mediterranean Sea. *Mar. Biol.* **1987,** 94, 271-275.
538 52. Sun, X.; Sun, S.; Ference, C.; Zhu, W.; Zhou, N.; Zhang, Y.; Zhou, K. A potent antimicrobial
539 compound isolated from Clathria cervicornis. *Bioorg. Med. Chem. Lett.* **2015,** 25, 67-69.
540 53. Rubiolo, J. A.; Ternon, E.; López-Alonso, H.; Thomas, O. P.; Vega, F. V.; Vieytes, M. R.; Botana, L.
541 M. Crambescidin-816 Acts as a Fungicidal with More Potency than Crambescidin-800 and -830,
542 Inducing Cell Cycle Arrest, Increased Cell Size and Apoptosis in Saccharomyces cerevisiae. *Mar. Drugs*
543 **2013,** 11, 4419-4434.
544 54. Kasmiati, K.; Yoshioka, Y.; Okamoto, T.; Ojika, M. New Crambescidin-Type Alkaloids from the
545 Indonesian Marine Sponge Clathria bulbotoxa. *Mar. Drugs* **2018,** 16, 84.
546 55. Campos, P. E.; Ferreira Queiroz, E.; Marcourt, L.; Wolfender, J. L.; Sanchez, A. S.; Illien, B.; Al
547 Mourabit, A.; Gauvin-Bialecki, A. Isolation and identification of new secondary metabolites from the
548 marine sponge Monanchora unguiculata. *Planta Med.* **2016,** 82, P580.
549 56. Campos, P.-E.; Wolfender, J.-L.; Queiroz, E. F.; Marcourt, L.; Al-Mourabit, A.; Frederich, M.;
550 Bordignon, A.; De Voogd, N.; Illien, B.; Gauvin-Bialecki, A. Unguiculin A and Ptilomycalins E–H,
551 Antimalarial Guanidine Alkaloids from the Marine Sponge Monanchora unguiculata. *J. Nat. Prod.* **2017,**
552 80, 1404-1410.
553 57. Lazaro, J. E. H.; Nitcheu, J.; Mahmoudi, N.; Ibana, J. A.; Mangalindan, G. C.; Black, G. P.; Howard-
554 Jones, A. G.; Moore, C. G.; Thomas, D. A.; Mazier, D.; Ireland, C. M.; Concepcion, G. P.; Murphy, P. J.;
555 Diquet, B. Antimalarial Activity of Crambescidin 800 and Synthetic Analogues against Liver and Blood
556 Stage of Plasmodium sp. *The Journal of Antibiotics* **2006,** 59, 583-590.

557 58. Takishima, S.; Ishiyama, A.; Iwatsuki, M.; Otoguro, K.; Yamada, H.; Omura, S.; Kobayashi, H.; van
558 Soest, R. W.; Matsunaga, S. Merobatzelladines A and B, anti-infective tricyclic guanidines from a marine
559 sponge Monanchora sp. *Org. Lett.* **2009,** 11, 2655-2658.
560 59. Suna, H.; Aoki, S.; Setiawan, A.; Kobayashi, M. Crambescidin 800, a pentacyclic guanidine
561 alkaloid, protects a mouse hippocampal cell line against glutamate-induced oxidative stress. *Journal of*
562 *Natural Medicines* **2007,** 61, 288-295.
563 60. Nakao, Y.; Fusetani, N. Enzyme Inhibitors from Marine Invertebrates. *J. Nat. Prod.* **2007,** 70, 689-
564 710.
565 61. Mai, S.; Nagulapalli, V.; Patil, A.; Truneh, A.; Westley, J. Marine compounds as HIV inhibitors. *US*
566 *Patent Application No. WO9301193 (A1)* **1993,** 21.
567 62. Patil, A. D.; Kumar, N. V.; Kokke, W. C.; Bean, M. F.; Freyer, A. J.; Brosse, C. D.; Mai, S.; Truneh,
568 A.; Carte, B. Novel alkaloids from the sponge Batzella sp.: inhibitors of HIV gp120-human CD4 binding.
569 *The Journal of Organic Chemistry* **1995,** 60, 1182-1188.
570 63. Bewley, C. A.; Ray, S.; Cohen, F.; Collins, S. K.; Overman, L. E. Inhibition of HIV-1 Envelope-
571 Mediated Fusion by Synthetic Batzelladine Analogues. *J. Nat. Prod.* **2004,** 67, 1319-1324.
572 64. Rinehart, K. L.; Jares-Erijman, E. A. Crambescidins: new antiviral and cytotoxic compounds from
573 the sponge Crambe crambe. In Google Patents: 1998.
574 65. Rinehart, K. L.; Shi, J.-G.; Sun, F. Crambescidin compounds. In Google Patents: 2000.
575 66. Chang; Whittaker, N. F.; Bewley, C. A. Crambescidin 826 and Dehydrocrambine A: New
576 Polycyclic Guanidine Alkaloids from the Marine Sponge Monanchora sp. that Inhibit HIV-1 Fusion. *J.*
577 *Nat. Prod.* **2003,** 66, 1490-1494.
578 67. Gustafson, K. R.; Oku, N.; Milanowski, D. J. Antiviral Marine Natural Products. *Current Medicinal*
579 *Chemistry - Anti-Infective Agents* **2004,** 3, 233-249.
580 68. Patil, A. D.; Freyer, A. J.; Taylor, P. B.; Carté, B.; Zuber, G.; Johnson, R. K.; Faulkner, D. J.
581 Batzelladines F–I, Novel Alkaloids from the Sponge Batzella sp.: Inducers of p56lck-CD4 Dissociation.
582 *The Journal of Organic Chemistry* **1997,** 62, 1814-1819.
583 69. Patil, A. D.; Freyer, A. J.; Offen, P.; Bean, M. F.; Johnson, R. K. Three New Tricyclic Guanidine
584 Alkaloids from the Sponge Batzella sp. *J. Nat. Prod.* **1997,** 60, 704-707.

70. Olszewski, A.; Sato, K.; Aron, Z. D.; Cohen, F.; Harris, A.; McDougall, B. R.; Robinson, W. E.; Overman, L. E.; Weiss, G. A. Guanidine alkaloid analogs as inhibitors of HIV-1 Nef interactions with p53, actin, and p56^{lck}. *Proc. Natl. Acad. Sci. U. S. A.* **2004,** 101, 14079-14084.

71. Hua, H.-M.; Peng, J.; Dunbar, D. C.; Schinazi, R. F.; de Castro Andrews, A. G.; Cuevas, C.; Garcia-Fernandez, L. F.; Kelly, M.; Hamann, M. T. Batzelladine alkaloids from the caribbean sponge Monanchora unguifera and the significant activities against HIV-1 and AIDS opportunistic infectious pathogens. *Tetrahedron* **2007,** 63, 11179-11188.

72. Van De Waterbeemd, H.; Gifford, E. ADMET in silico modelling: towards prediction paradise? *Nature reviews Drug discovery* **2003,** 2, 192-204.

73. Mannhold, R.; Kubinyi, H.; Folkers, G. *Pharmacokinetics and metabolism in drug design*. John Wiley & Sons: 2012; Vol. 51.

74. Klopman, G.; Stefan, L. R.; Saiakhov, R. D. ADME evaluation: 2. A computer model for the prediction of intestinal absorption in humans. *European journal of pharmaceutical sciences* **2002,** 17, 253-263.

75. Roy, P. P.; Roy, K. QSAR studies of CYP2D6 inhibitor aryloxypropanolamines using 2D and 3D descriptors. *Chemical biology & drug design* **2009,** 73, 442-455.

76. Ghafourian, T.; Amin, Z. QSAR models for the prediction of plasma protein binding. *BioImpacts: BI* **2013,** 3, 21.

77. Xia, X.; Maliski, E. G.; Gallant, P.; Rogers, D. Classification of kinase inhibitors using a Bayesian model. *Journal of medicinal chemistry* **2004,** 47, 4463-4470.

78. BIOVIA. QSAR, ADMET and Predictive Toxicology. https://www.3dsbiovia.com/products/collaborative-science/biovia-discovery-studio/qsar-admet-and-predictive-toxicology.html (May 2020).

79. Venkatapathy, R.; Wang, N. C. Y.; Martin, T. M.; Harten, P. F.; Young, D. Structure–Activity Relationships for Carcinogenic Potential. *General, Applied and Systems Toxicology* **2009**.

80. Goodrnan, G.; Wilson, R. Comparison of the dependence of the TD50 on maximum tolerated dose for mutagens and nonmutagens. *Risk Analysis* **1992,** 12, 525-533.

612 81. Council, N. R. Correlation Between Carcinogenic Potency and the Maximum Tolerated Dose:
613 Implications for Risk Assessment. In *Issues in Risk Assessment*, National Academies Press (US): 1993.
614 82. Gonella Diaza, R.; Manganelli, S.; Esposito, A.; Roncaglioni, A.; Manganaro, A.; Benfenati, E.
615 Comparison of in silico tools for evaluating rat oral acute toxicity. *SAR and QSAR in Environmental*
616 *Research* **2015,** 26, 1-27.
617 83. Pizzo, F.; Benfenati, E. In silico models for repeated-dose toxicity (RDT): prediction of the no
618 observed adverse effect level (NOAEL) and lowest observed adverse effect level (LOAEL) for drugs. In
619 *In Silico Methods for Predicting Drug Toxicity*, Springer: 2016; pp 163-176.
620 84. Venkatapathy, R.; Moudgal, C. J.; Bruce, R. M. Assessment of the oral rat chronic lowest observed
621 adverse effect level model in TOPKAT, a QSAR software package for toxicity prediction. *Journal of*
622 *chemical information and computer sciences* **2004,** 44, 1623-1629.
623 85. Harvey, A. L. Presynaptic effects of toxins. *International review of neurobiology* **1990,** 32, 201-39.
624 86. El-Gamal, K. M.; El-Morsy, A. M.; Saad, A. M.; Eissa, I. H.; Alswah, M. Synthesis, docking, QSAR,
625 ADMET and antimicrobial evaluation of new quinoline-3-carbonitrile derivatives as potential DNA-
626 gyrase inhibitors. *Journal of Molecular Structure* **2018,** 1166, 15-33.
627 87. Li, N.; Wang, Y.; Li, W.; Li, H.; Yang, L.; Wang, J.; Mahdy, H. A.; Mehany, A.; Jaiash, D. A.; Santali,
628 E. Y. Screening of Some Sulfonamide and Sulfonylurea Derivatives as Anti-Alzheimer's Agents
629 Targeting BACE1 and PPARγ. *Journal of Chemistry* **2020,** 2020.
630 88. Ibrahim, M. K.; Eissa, I. H.; Alesawy, M. S.; Metwaly, A. M.; Radwan, M. M.; ElSohly, M. A. Design,
631 synthesis, molecular modeling and anti-hyperglycemic evaluation of quinazolin-4 (3H)-one derivatives
632 as potential PPARγ and SUR agonists. *Bioorganic & medicinal chemistry* **2017,** 25, 4723-4744.
633 89. Elmetwally, S. A.; Saied, K. F.; Eissa, I. H.; Elkaeed, E. B. Design, synthesis and anticancer
634 evaluation of thieno [2, 3-d] pyrimidine derivatives as dual EGFR/HER2 inhibitors and apoptosis
635 inducers. *Bioorganic chemistry* **2019,** 88, 102944.
636 90. Mahdy, H. A.; Ibrahim, M. K.; Metwaly, A. M.; Belal, A.; Mehany, A. B.; El-Gamal, K. M.; El-
637 Sharkawy, A.; Elhendawy, M. A.; Radwan, M. M.; Elsohly, M. A. Design, synthesis, molecular
638 modeling, in vivo studies and anticancer evaluation of quinazolin-4 (3H)-one derivatives as potential
639 VEGFR-2 inhibitors and apoptosis inducers. *Bioorganic Chemistry* **2020,** 94, 103422.

640 91. El-Zahabi, M. A.; Elbendary, E. R.; Bamanie, F. H.; Radwan, M. F.; Ghareib, S. A.; Eissa, I. H.
641 Design, synthesis, molecular modeling and anti-hyperglycemic evaluation of phthalimide-sulfonylurea
642 hybrids as PPARγ and SUR agonists. *Bioorganic chemistry* **2019,** 91, 103115.
643 92. El-Naggar, A. M.; Eissa, I. H.; Belal, A.; El-Sayed, A. A. Design, eco-friendly synthesis, molecular
644 modeling and anticancer evaluation of thiazol-5 (4 H)-ones as potential tubulin polymerization
645 inhibitors targeting the colchicine binding site. *RSC Advances* **2020,** 10, 2791-2811.
646